

Development of Multimodal Quantitative MRI Techniques to Assess Brain Tissue Microstructure in Multiple Sclerosis

Mathieu Boudreau

Supervisor: Bruce Pike

PhD Progress Meeting

Biomedical Engineering Department

McGill University

FINAL - 12/11/14 9:28 PM

1. Introduction and Objectives

Multiple sclerosis (MS) is arguably the most disabling chronic neurological disease affecting a sizable portion of young adult Canadians. While the trigger of the disease is still unknown, considerable efforts have been made in the last few decades at investigating the progression of the pathology of MS. Magnetic resonance imaging (MRI) has emerged as an important imaging modality for diagnosing MS by detecting MS lesions and, in some instances, measuring multiple aspects of the disease. Some techniques provide mostly qualitative features such as T₂ weighted images, but more recently quantitative measures of myelin and water content have been achieved with novel MRI techniques such as quantitative magnetization transfer (qMT) imaging and quantitative T₂. Until now, most of the effort at characterizing MS with MRI has concentrated on white matter (WM) pathology, but recent post-mortem studies have emphasized the importance of cortical grey matter (GM) pathology to fully characterize the disease. **In this thesis, we aim to develop a fast high-resolution whole-brain quantitative magnetization transfer method capable of characterizing white and gray matter MS pathology.**

2. Abbreviated Literature Review

2.1 Multiple Sclerosis

Canada has one of the highest occurrences of MS in the world. MS occurs mostly in women, with clinical onset typically beginning between ages 15-40 (1) and burdens the patient for their entire lifetime. MRI plays a crucial role in the diagnosis of MS, as described by the McDonald Criteria (last revised in 2010) (2). The most common type of MS is conventionally characterized as intermittent attacks of focal WM inflammation and demyelination (plaques), separated by periods of relative stability (3-5). Demyelination in MS WM is believed to be a result of an immunologically mediated attack on myelin and oligodendrocytes (4). Although MS has mostly been described as a WM disease, post-mortem histological evidence has shown many abnormalities in cortical GM of MS patients (6,7). GM lesions are characterized by demyelination, axonal and dendritic transection, neuronal apoptosis and limited inflammatory cell content compared to WM lesions (8-12). One post-mortem study observed that 26% of MS lesions involved some GM (13). Another recent study reported that cortical GM pathology significantly correlated with neurological impairment in relapse-remitting MS patients (14). Despite this, most MRI techniques currently in use concentrate on WM lesions. The development of MRI methods capable of quantifying cortical GM pathology is important to fully characterize MS.

2.2 Magnetic Resonance Imaging of MS

MRI is well known to be very sensitive to various pathologies related to MS (2,7,15-21). The conventional MRI characteristic of MS is hyperintense signals in T₂-weighted MRI of multiple focal WM lesions. However, T₂ hyperintensity has little specificity to the lesion environment, as multiple pathological changes such as acute inflammation and axonal loss can lengthen T₂. Conventional MRI also does not detect the full extent of MS pathology in regions referred to as normal appearing white matter (NAWM) and cortical GM. Brain atrophy, a common disease progression indicator for many neurological diseases such as MS, can also be quantified using MRI (14,22-25).

Cortical GM lesions typically elude MRI detection with clinical MRI scans (26,27). New techniques such as double inversion recovery (DIR) have shown better detection of cortical lesions. DIR uses two inversion pulses that null both WM and CSF, ideally leaving mostly GM signal (28). However, low SNR and CNR of DIR limit the detection of subtle cortical lesions.

2.3 Quantitative MRI

Quantitative MRI techniques, such as quantitative T₁, T₂, diffusion, and magnetization transfer, have become the focus of research development for MS due to their promise of providing hardware and site independent MRI measures and better MS diagnostic specificity (29). MT measures have been shown to strongly correlate with myelin content in brain white matter (16,17), and it is expected that a similar correlation with grey matter can be observed if resolution and SNR is improved (20).

2.4 Magnetization Transfer

Magnetization transfer (MT) is the MR phenomenon of nuclear spins in different environments exchanging magnetization through coupled relaxation (30-33). This method provides an indirect measurement of hydrogen in a semi-solid macromolecular state, as signal from these molecules is undetected with conventional MRI due to the characteristic fast signal decay of solids. This technique provides an indirect measurement of relative semi-solid (e.g. myelin) density. Although MT has been mostly used to investigate multiple sclerosis, other applications include HIV (34-36), Alzheimer's disease (37-40), and articular cartilage (41,42).

The most simple and common magnetization transfer metric is the magnetization transfer ratio (MTR), which consists of two measurements: one with and one without an off-resonance saturation pulse. Although MTR has been shown to correlate with T₁/T₂ weighted MRI images and histology (16), quantitative methods using mathematical models of the magnetization transfer (31,43-47) can provide a more quantitative analysis of the disease. Schmieder et al. (17) compared qMT measurements with quantitative histology on post-mortem MS brains and observed that myelin density was strongly correlated with the restricted pool size ratio (F), and that F could distinguish between normal appearing WM and remyelinated WM lesions; however, cortical pathology was not examined. qMT MRI protocols have historically suffered from very long acquisition times due to the large number of measurements typically required. Several developments have been introduced to overcome this limitation, such as optimal sampling schemes (48,49), reduced sampling by parameter restricting (50,51) and novel qMT re-interpretations of rapid pulse sequences (52).

2.5 Compressed Sensing

Compressed sensing is an image compression technique whose underlying principles have recently been applied to MRI to accelerate image acquisition (53). It allows k-space data to be sampled below the Nyquist criteria while preserving image fidelity and SNR, and does not require major changes to MRI pulse sequence or new hardware. The basic idea behind compressed sensing is the following: **sparse signals may be accurately reconstructed from random k-space undersampling by solving a non-linear optimization problem.** There has been a rapid growth of the use of compressed sensing in the MRI community, with applications ranging from angiography (53), cardiac imaging (54) and diffusion spectrum imaging (55). Several model-based compressed sensing methods have been introduced to take advantage of sparsity in the parameter acquisition domain (56-58). Bayesian analysis has also been used for simultaneous multi-contrast compressed-sensing reconstruction (59,60). Lastly, an important branch of compressed sensing is the development of methods for multi-coil receivers (61-69).

3. Thesis Hypotheses

The major limitations to widespread use of the Sled and Pike qMT method is its very long acquisition times and single-slice acquisition. The low resolution of the protocol (2x2x7 mm³) also limits the confidence in cortical pathology measurements using this method. *The next logical step is to*

develop a high-resolution whole-brain 3D qMT protocol able to confidently characterize cortical pathology in addition to white matter so that fundamental questions on the spatial progression of pathology in MS may be answered.

To achieve this goal, I worked on two projects complimentary to Aim 1 (development of fast hi-resolution qMT) of the thesis hypotheses described in my 2012 project proposal. Results from these projects were presented at an international conference (ISMRM 2014, Milan, Italy), and received positive feedback. Following discussions with my thesis advisor (Dr. Bruce Pike) after the meeting, and some additional work over the course of the summer, we came to the mutual conclusions that this work warrants being reported as manuscripts. As such, due to the time invested on these projects, we decided to revise the proposed papers for the overall thesis. Nevertheless, the overall goal of the thesis presented above has not changed. Previously hypothesized Aims 2 (high-resolution post-mortem qMT of grey matter) and 3 (in-vivo diffusion and high resolution qMT in SPMS) have been removed from the PhD thesis proposal. Our research plan is now driven by the following hypotheses/questions:

1. *Comparing quantitative transmit radiofrequency field (B_1) mapping methods for whole-brain variable flip angle T_1 maps*

Due to an increased interest in acquiring quantitative MRI measures (e.g. T_1 , qMT) with whole brain coverage, several novel rapid B_1 mapping methods have gained considerable interest in the qMRI field. We present a comparison between the conventional double angle (DA) B_1 method, two novel methods (Bloch-Siegert (BS), Actual Flip Angle Imaging (AFI)), and a k-space accelerated (EPI) DA method using a stock scanner sequence. Results show that all B_1 sequences are adequate at producing comparable WM VFA T_1 maps, with their variability well below that observed between T_1 methods (70). Due to its easy implementation, k-space (EPI) accelerated DA B_1 mapping using stock sequences should be considered as an important alternative to novel methods.

2. *An analysis of the B_1 -sensitivity of qMT parameters*

For pulsed spoiled gradient echo (SPGR) qMT imaging experiments, B_1 maps are used as a corrective factor for the excitation flip angle and MT saturation power. T_1 mapping, also required for SPGR qMT, may require B_1 maps as a corrective factor; variable flip angle (VFA) T_1 mapping requires B_1 maps, while inversion recovery (IR) does not. Thus, local (e.g. artifacts) or global (e.g. systemic biases) inaccuracies in B_1 mapping will propagate to the fitted qMT parameters differently, depending on the chosen T_1 mapping method. This work explores the sensitivity of qMT parameters to B_1 inaccuracies through simulations and measurements at 3T using healthy subjects and an MS patient. We show that the pool-size ratio F is much more robust to B_1 inaccuracies when using VFA, as opposed to IR. Thus, lower resolution B_1 maps can be acquired (possibly even omitted) if VFA T_1 mapping is used.

3. *Quantitative MT acquisitions can be optimized for both white and grey matter sensitivity over the whole brain with a resolution of 1 mm³ in a clinically acceptable time of <30 minutes.*

Our current qMT protocol is based on a single-slice spoiled gradient echo (SPGR) sequence with many MT pulse power/offset/frequency/repetition time combinations. We will optimize our method for high resolution (1 mm³) whole-brain measurements at 3 T using a 32-channel head coil, optimal sampling scheme for normal/MS tissue properties at 3 T, and a novel compressed sampling imaging method to undersample k-space without losing integrity of the qMT maps. Comparisons between two compressed sampling methods and parallel imaging will be evaluated for efficiency in accelerating imaging and artifacts, and a whole-brain MS patient dataset will be acquired using this protocol.

4. Thesis Work Progress

4.1 Quantitative Comparison of B_1 Mapping Methods for White Matter T_1 Mapping at 3T (90% complete)

Introduction: The aim of this work was to compare VFA T_1 maps in white matter (WM) produced with four B_1 methods: Reference double angle (DA), Bloch-Siebert, Actual Flip-Angle Imaging, and DA using a stock scanner spin-echo EPI readout sequence (EPI-DA).

Methods: Prior to acquiring a set of subject data, several technical developments were made. Quantitative maps (B_1 , T_1) processing code were standardized and integrated into an automated Matlab pipeline using MINC and Niak. The Bloch-Siebert sequence was updated to use off-resonance Fermi pulse, in accordance with the parameters reported in the original paper (71). To investigate the white matter T_1 , a majority voting analysis resampling script was developed to resample high-resolution tissue classification maps (WM, GM, CSF- provided via INSECT with the ICBM-152 atlas) to the low resolution ($2 \times 2 \times 5 \text{ mm}^3$) B_1/T_1 maps.

Six healthy adult subjects were scanned with a 3T Siemens Tim Trio MRI using a 32-channel receive-only head coil. Axial slices ($2 \times 2 \times 5 \text{ mm}^3$) were acquired (or extracted from 3D volumes) parallel to the AC-PC line above the corpus callosum. Quantitative analyses were done on the unfiltered (raw) B_1 maps. The raw B_1 maps were also filtered (Gaussian blurring and spline smoothing) for qualitative comparison (Fig. 4).

Results: To determine how each B_1 maps compared in producing WM T_1 maps, a single slice was extracted and masked for WM tissue for each subject prior to histogram and statistical analysis. We observed very little differences in overall WM T_1 distribution when comparing against each B_1 methods (Fig. 1). The largest deviation in T_1 (mode) relative to the Reference DA B_1 map was for EPI-DA (4% decrease). This deviation is substantially lower than those reported between T_1 methods (IR, VFA, Look-Locker), which can vary up to 30% (70).

Each B_1 methods are based off different pulse sequences (Ref. DA: spin-echo with full magnetization recovery, AFI: steady state, Bloch-Siebert: phase-based, EPI DA: fast k-space trajectory), which make them uniquely sensitive to different artifacts. Visual inspection of the B_1 maps shows distinctive artifacts for our implementations of each method (Fig. 2a (bottom) and Fig. 4). No significant B_1 maps distortions were observed in a sagittal EPI-DA B_1 maps (Fig. 3).

Linear regression analysis of pooled WM T_1 for each B_1 relative to the reference is shown in Figure 5. The WM T_1 produced by all rapid B_1 methods correlated strongly (>0.97) with the Ref. DA. EPI-DA, the fastest of the B_1 maps (5 s/slice), had no observable distortion artefacts (Figs. 2 and 3), due to careful sequence planning (low EPI factor, long echo spacing).

Manuscript Progress: An initial draft the manuscript (technical report, Mag. Res. Med) is in progress, and will be distributed to the co-authors within a few weeks.

4.2 B_1 -Sensitivity Analysis of qMT (80% Complete)

Introduction: Quantitative magnetization transfer (qMT) imaging requires several additional measurements to correct for instrumental biases (B_0 , B_1) and to constrain parameters in the fitting model (T_1). These three extra measurements are typically independent of each other, but certain T_1 mapping techniques also require B_1 maps (e.g. variable flip angle – VFA). In this case, B_1 is used twice before fitting the qMT parameters: to correct the flip angles for T_1 mapping, and to scale the nominal MT saturation powers. Inaccuracies in B_1 would propagate to the fitting of the qMT parameters through two pathways – through errors induced in T_1 , and errors in MT saturation powers. This work

demonstrated that for the Sled and Pike SPGR qMT model, the pool-size ratio F much less sensitive B_1 inaccuracies when using VFA for T_1 mapping.

Methods and Results: This study is separated into five stages to investigate the sensitivity of B_1 inaccuracies on qMT parameters.

1. *Noiseless simulation of single tissue qMT for B_1/T_1 inaccuracies*
2. *B_1 -sensitivity of qMT parameters in-vivo*
3. *Comparison using 3 B_1 mapping methods*
4. *B_1 -sensitivity of qMT parameters in pathology: RRMS patient*
5. *Insights on the origin of the qMT F B_1 -insensitivity*

Stage 1: The Bloch-McConnell equations for magnetization exchange were solved using MATLAB for a pulsed SPGR. Healthy white matter tissue parameters were fixed to normal values for 3T. The MT signal was simulated from the solution of the Bloch-McConnell equation for the uniform MT protocol (49). The MT signal was subsequently fitted using the Sled and Pike method for a linear range of 100 B_1 and 100 T_1 values. B_1 ranged from 0.5 to 2 ($B_{1,\text{true}} = 1$), and T_1 ranged from 0.1 s to 4 s ($T_{1,\text{true}} = 0.9$ s). Results are shown in Figs. 6 and 7. Errors in F induced by B_1 errors were greatly reduced using VFA T_1 mapping (Fig. 7a). This work recently was submitted as an abstract to ISMRM (Appendix 2).

Stage 2: Three healthy adults were scanned with a 3T Siemens Tim Trio MRI using a 32-channel receive-only head coil. VFA and IR T_1 maps were acquired. qMT data was acquired using the spoiled gradient echo two-TR uniform 10-point protocol for 3T (49). A double angle spin echo B_1 map was acquired. To simulate B_1 inaccuracies for a broader range of tissue values than Stage 1 (single tissue), flat (homogenous) B_1 maps were produced, ranging from 0.5 to 2. VFA T_1 maps and corrected MT saturation powers were then calculated from these flat B_1 . Note that VFA T_1 calculated with a flat B_1 factor of 1 is equivalent to fitting VFA T_1 maps using the nominal flip angles. qMT maps were fitted with B_1 maps using DA and flat B_1 , as well as IR T_1 maps and VFA T_1 maps. Whole-brain voxel data from all subjects were pooled for each qMT/ T_1/B_1 sets, and linear regressions and correlations were calculated between B_1 DA and every B_1 Flat maps. Results are shown in Figs 8, 9, 10 and 11.

Stage 3: In addition to using the data acquired in Stage 2, two additional B_1 maps were acquired (Bloch-Siegert Shift (71), Actual Flip Angle Imaging (72,73)). The qMT maps were fitted for all three acquired B_1 maps (unfiltered), using both VFA and IR B_1 maps, and masked for WM in a similar procedure described in Section 4.1.

Figure 12 shows the histograms of WM F and kf, for VFA and IR. It can be clearly seen that the histograms of F values match best between all three B_1 maps (prone to local inaccuracies, see Figs. 2 and 4) when using VFA. In agreement with simulations from Step 1 (Fig. 7b), better matching of the kf histograms occurs when using IR.

Stage 4: A fully acquired whole brain ($2 \times 2 \times 2$ mm 3) qMT data set (similar the one described in Step 2) of an MS patient was acquired in early December 2013 by two Pike lab members (Dr. Nikola Stikov and Dr. Jennifer Campbell), the data was generously be shared with me. The patient is a 38-year-old male subject with definite relapse-remitting MS (RRMS), EDSS 3.0. Analysis of this data is still a work in progress.

Stage 5: An approximate sensitivity analysis was implemented using simulations (Figure 13). Comparing the sensitivity of both MT flip angles in the case of B_1 errors using IR T_2 (Fig. 13a) and VFA T_1 (13b), it's clear that F will be very stable in the fit for the case of VFA T_1 , as any changes in F requires induces large changes in both MT angles Z-spectrums. The sensitivity of the exchange rate kf matches that of the VFA case, thus errors induced by B_1 can be nearly completely compensated from this variable.

Conclusion: The overall results of this work implies that B_1 mapping may be completely eliminated from our qMT protocol by using VFA for T_1 maps with no substantial biases on F, which could save up to 5-10 minutes from our 3D qMT protocol acquisition time.

4.3 Analytical qMT Sensitivity Analysis (10% Complete, optional)

Several methods of analyzing the source of the B_1 -insensitivity discussed in the previous section were explored – including a possible collaboration with Stephen Cauley (Harvard). I decided to pursue a system sensitivity analysis method (74), and a derivation for analytically analyzing the B_1 -sensitivity of qMT imaging is described briefly in Appendix A. I believe that a comprehensive analysis of this type is out of the scope of the paper proposed in Section 4.3, but is indicated as being optional here in the case a reviewer requests its inclusion.

4.4 qMT Compressed Sensing (20% Complete)

The compressed sensing k-space acceleration project is still a work in progress. Sparse k-space pulse sequence acquisition was developed with Raphaël Paquin (Siemens scientist). The method was successfully developed to the stock Siemens 2D gradient echo pulse sequence (the base sequence for our qMT sequences), with the capability of reading the k-space lines to be acquired from a text file, allowing for great at-the-scanner flexibility. This feature needs to be extended to 3D and merged with our qMT sequence. To aid in this transition, an additional feature to the qMT sequence was developed to allow single point acquisitions instead of full qMT protocols, and user interface MT parameter control (MT saturation, off-resonance frequency). Additionally, as raw (k-space) data from all 32 channels must be used for compressed sensing, Matlab code was developed to organize the loaded raw data into k-space and/or image domain matrices using the measurement data headers. Lastly, an open source L₁-SPIRIT (61,63) multi-channel sparse acquisition image reconstruction software package was installed and tested on one of our lab computers. This software significantly accelerates multi-channel L1-Spirit processing through the use GPU processing or OpenMP multi-processor tools. . Raw single slice (2x2x5 mm³) k-space data (fully acquired) of our optimal 10-point qMT protocol has been acquired for 5 healthy subjects as part of another study (Sections 4.1 and 4.2). This data set will be helpful in evaluating compressed sensing artefacts that may result in the loss of lesion information in fitted qMT maps.

4.5 Other – 2014 Training and Collaborations

Throughout this year, I had the opportunity to participate in several training opportunities. The abstract submitted for the 2013 endMS conference was accepted, and I was awarded a scholarship covering the complete cost of attending the conference in Saint-Sauveur. This conference was a great opportunity to network and discuss with interdisciplinary Canadian MS researchers, and contained many trainee-oriented sessions (e.g. a communication workshop by the Alan Alda Center for Communicating Science). Both abstracts submitted last year for the 2014 ISMRM meeting were also accepted: a traditional poster and an electronic poster. I was awarded an ISMRM Trainee Educational Stipend to attend the meeting in Milan and the weekend educational course that preceded the meeting. Throughout the year, I attended several endMS Network workshop organized at the MNI, such as the four-session endMS Statistics Series. I also attend and a Software Carpentry workshop in January (Montreal), and the 2014 MS Exchange conference November (Montreal).

Following the gradual departure of Ye Gu and Dr. Nikola Stikov from our lab, my experience with acquiring and processing qMT data allowed me to collaborate with many local and international researchers. I acquired and analyzed a whole-brain RRMS data set for Dr. Nikola Stikov and Dr.

Jennifer Campbell (Montreal Neurological Institute), and was granted co-authorship in a recently submitted manuscript (Appendix D). Dr. Stikov also requested my assistance for preliminary data for a research grant application in collaboration with Dr. Julien Cohen-Adad (Polytechnique Montreal). Over several months, I was involved with planning, acquiring, and analyzing qMT data in pig and cat spinal cords on our human 3T MRI at the MNI, and the animal 7T scanner at the Montreal Heart Institute. Co-authorship was not attributed in any conference abstracts or papers for my assistance in this project. I provided technical assistance and troubleshooting to Dr. Jacqueline Chen (Lerner Research Institute, Cleveland, Ohio) regarding the implementation of an AFI B_1 mapping acquisition and analysis on their 3T Siemens scanner. At the request of Dr. Stikov, I explored a possible collaboration with Dr. Aviv Mezer (Stanford University) involving the efficacy of fitting the MT exchange rate k_f by fixing F in the model using his macromolecular tissue volume biomarker for myelin (75). I assisted Dr. David Rudko and Dr. Robert Brown (Montreal Neurological Institute) with acquiring and analyzing qMT data using our qMT software. I am currently in an on-going collaboration with Melany Ann McLean (University of Calgary, Dr. Pike's lab), assisting with qMT data analysis development for a small animal project.

5. Thesis Completion Plan

5.1 First Thesis Paper: *Quantitative Comparison of B_1 Mapping Methods for White Matter T_1 Mapping at 3T*

This project is near completion. The manuscript is already in progress, and no additional measurements are expected prior to submission of this work.

5.2 Second Thesis Paper: *B_1 -Sensitivity Analysis of qMT*

This project is also near completion. Only minor analysis work of the MS patient data is left to do prior to submission. No additional measurements are expected prior to submitting the manuscript.

5.3 Third Thesis Paper: *Analytical Analysis of B_1 -Sensitivity of Quantitative Magnetization Imaging*

A sensitivity analysis (74) derivation for analytically analyzing the B_1 -sensitivity of qMT imaging is described briefly in Appendix A. Sensitivity analyses will be evaluated for several established qMT imaging protocols, using the B_1 -independent T_1 assumption as well as VFA T_1 . The analytical solution of the pulsed qMT sequence under established assumptions will be used for the sensitivity analysis. The effects on the B_1 -sensitivity of constraining certain parameters, as have been recently proposed (50), will be explored. Lastly, the possibility of optimizing the qMT acquisition protocol for minimum B_1 -sensitivity will be explored, with the aim of achieving a qMT protocol without a B_1 map.

5.4 Fourth Thesis Paper: *Accelerated qMT Using Compressed Sensing*

The next step in the completion of the final paper of this thesis will be to establish a compressed sensing image reconstruction technique for our qMT pulse sequence. This may involve a collaboration with Dr. Ives Levesque, an alumni of Dr. Pike's lab, and a medical imaging physicist who has recently joined McGill University as an assistant professor at the McGill University Health Center.

The first step will be to investigate the sensitivity of each qMT Z-spectrum acquisitions to compressed sensing related artifacts that propagate into the final qMT fitted parameter maps. This will be investigated using the open source L_1 -SPIRiT+Wavelet reconstruction processing code mentioned in Section 4.4. K-space data will be retroactively undersampled at different acceleration factors for each qMT point, then each point will be individually reconstructed and fitted for qMT parameters with

the other fully sampled qMT points.

Once the L₁-SPIRiT qMT acquisition sensitivity has been established, an alternative compressed sensing method developed for quantitative parameter mapping using locally low rank constraints (76), will be evaluated for qMT and compared to our L₁-SPIRiT analysis. This method takes advantage of the data redundancy in the MRI parameter domain (e.g. for T₂ measurements, the parameter being varied is TE) through sparsity in the singular values of a Casorati matrix (column is the image voxel dimension, row is the parameter dimensions). This method is a model-free parameter-domain compressed sensing method, and may promise to be more efficient at accelerating acquisition than the L₁-Spirit method, which does not take into account of parameter domain redundancy. The comparison and optimization of these two methods qMT (and possibly parallel imaging acceleration) using will be written as a full paper.

6. Timeline for Completion of Thesis

6.1 January 2014–February 2015

The overall thesis completion timeline is shown in Fig. 14. The first thesis paper (“*A Comparison of B₁ Mapping Methods for T₁ Mapping at 3T*”) has already been in the writing process and is nearing completion of the first draft. I anticipate distributing a draft to co-authors by mid-January. While it circulates for corrections, I will write the second thesis paper (“*B₁-Sensitivity Analysis of qMT*”), which only minor data analysis in a section remains. My aim is to submit both these papers by March 2015.

6.2 March 2015 - September 2015

The optional third paper (Section 8 - Chapter 5, *Analytical B₁ Sensitivity Analysis of qMT*) will be worked on over the following six months, but priority will be given to the final and fourth paper. This work will only result in its own manuscript if the reviewers for our second manuscript (Section 8, Chapter 4) do request its inclusion in that manuscript.

The target completion date for the final (fourth paper) is September 2015. March 2015 and April 2015 will be spent investigating the qMT Z-spectrum point sensitivity on retroactive compressed sensing reconstruction. Healthy subject data (N = 5) has already been acquired, and multi-coil L₁-Spirit GPU reconstruction code is already openly available and will be used. If possible, compressed sensing reconstructions effect on lesions will be explored with raw qMT data of a few RRMS and/or SPMS MS patients that may have been collected by Dr. David Rudko, a post-doctoral fellow in Dr. Arnolds lab, if the data is available. Locally low rank (LLR) sparsity reconstruction for parameter MRI mapping will be evaluated for qMT in May and June 2015. Both LLR and L₁-SPIRiT will be compared in a small in vivo investigation using a whole-brain qMT data set of healthy subjects in July and August 2015.

6.3 October 2015 - December 2015

The final and fourth research paper will be written and submitted by December 2015. The remaining thesis chapters (Introduction, Background, Conclusion) will also be written between October and December 2015. My goal is to submit my PhD thesis by the December 15th 2015 term deadline.

7. PhD Publications and Conference Proceedings

7.1 Published Manuscripts

1. Nikola Stikov, **Mathieu Boudreau**, Ives Levesque, Christine Tardif, Joëlle Barral, G. Bruce Pike, “*On the Accuracy of T₁ Mapping: Searching for Common Ground*”, Magnetic Resonance in Medicine, DOI: 10.1002/mrm.25135 (2014)

7.2 Submitted Manuscripts

1. Nikola Stikov, Jennifer S.W. Campbell, Thomas Stroh, Stephen Frey, Jennifer Novek, Stephen Nuara, Ming-Kai Ho, Barry J. Bedell, Robert F. Dougherty, Ilana R. Leppert, **Mathieu Boudreau**, Sridar Narayanan, and G. Bruce Pike, “*In vivo histology of the myelin g-ratio with magnetic resonance imaging*”, Neuroimage, (Submitted on: December 5th 2014)

7.3 Manuscripts in Progress

1. **Mathieu Boudreau**, Christine Tardif, Nikola Stikov, G. Bruce Pike, “*A Comparison of B_1 Mapping Methods for T_1 Mapping at 3T*”, Proposed submission to: Magnetic Resonance in Medicine, Format: Technical Note (2015)
2. **Mathieu Boudreau**, Nikola Stikov, Douglas L. Arnold, G. Bruce Pike, “ *B_1 -Sensitivity Analysis of qMT*”, Proposed submission to: Magnetic Resonance in Medicine, Format: Full Paper (2015)

7.4 Proposed Manuscripts

1. **Mathieu Boudreau**, Nikola Stikov, Stephen Cauley, G. Bruce Pike, “*Analytical Analysis of B_1 -Sensitivity of Quantitative Magnetization Imaging*”, Proposed submission to: Medical Physics, Format: Technical Note (2015)
2. **Mathieu Boudreau**, Ives R. Levesque, David Rudko, Tao Zhang, Douglas L. Arnold, G. Bruce Pike, “*Optimized Acceleration of Quantitative Magnetization Transfer Parameter Mapping Using Locally Low Rank Sparsity*”, Proposed submission to: Magnetic Resonance in Medicine, Format: Full Paper (2015)

7.5 Peer Reviewed Conference Abstracts

1. N. Stikov, J. Campbell, **M. Boudreau**, S. Narayanan, T. Stroh, S. Nuara, J. Novek, S. Frey, M.-K. Ho, B. Bedell, G. B. Pike, “*In vivo histology of the myelin g-ratio*”, Poster, OHBM Annual Meeting (2014)
2. **Mathieu Boudreau**, Nikola Stikov, G. Bruce Pike, “*A B_1 Insensitive qMT Protocol*”, Poster, International Society for Magnetic Resonance in Medicine Meeting (2014)
3. **Mathieu Boudreau**, Christine Tardif, Nikola Stikov, G. Bruce Pike, “*A Comparison of B_1 Mapping Methods for T_1 Mapping at 3T*”, E-Poster, International Society for Magnetic Resonance in Medicine Meeting (2014)
4. **Mathieu Boudreau**, Nikola Stikov, G. Bruce Pike, “*Effect of Different T_1 Mapping Techniques on a Quantitative Magnetization Transfer MRI Biomarker for Myelin Density*”, Poster, endMS Conference (2013)
5. **Mathieu Boudreau**, Nikola Stikov, G. Bruce Pike, “ *T_1 Mapping: Should We Agree To Disagree?*”, Poster, International Society for Magnetic Resonance in Medicine Meeting (2013)

7.6 Submitted Conference Abstracts

1. **Mathieu Boudreau**, Nikola Stikov, G. Bruce Pike, “ *B_1 -Sensitivity Analysis of qMT*”, Submitted to: International Society for Magnetic Resonance in Medicine Meeting 2015
2. Ye Gu, **Mathieu Boudreau**, Ives R Levesque, Yaaseen Atchia, John Sled, Sridar Narayanan, Douglas L. Arnold, Bruce Pike, and Nikola Stikov, “*Quantitative Magnetization Transfer Analysis: An Interactive Introduction with qMTLab*”, Submitted to: International Society for Magnetic Resonance in Medicine Meeting 2015

8. Thesis Draft Outline

Chapter 1: Introduction

Motivation for the thesis work will be introduced in Chapter 1. Broad facts about the current knowledge of MS will be discussed at a level accessible to non-experts. Previous MRI limitations

leading to the technical developments of this thesis will be discussed. The broad aim of this thesis will be stated.

Chapter 2: Background

Chapter 2 will cover the background required to understand the following integrated articles at level accessible to MS and MRI researchers. White matter MS pathology will be discussed, following by the current state of knowledge of cortical grey matter MS pathology. An overview of the current state of quantitative MRI techniques (B_0 , B_1 , and T_1) will be presented. Quantitative magnetization transfer MRI will be explained in detail, and relevant recent studies will be presented. The compressed sensing technique will be described in detail, and a comparison between methods will be presented.

Chapter 3: (Integrated article, Technical Note) $qMT B_1$ Insensitivity when using VFA T_1 Maps

Chapter 3 will contain the *published* journal article presenting a comparison of B_1 techniques and their application to VFA T_1 mapping. The audience of the paper will be researchers seeking to integrate whole brain B_1 mapping in their study protocols. The main aim of this paper is to demonstrate that k-space (EPI) double angle B_1 imaging is a sufficient alternative to recent novel B_1 methods for whole brain imaging, and correlates better to the reference double angle B_1 method. A short discussion on filtering B_1 maps will be presented.

Chapter 4: (Integrated article, Full Paper) B_1 -Sensitivity Analysis of qMT

Chapter 4 will contain the *published* journal article presenting an analysis of the B_1 sensitivity of qMT parameters under two regimes: B_1 -independent T_1 mapping (e.g. IR) and B_1 -dependent T_1 mapping (e.g. VFA). Simulations will be presented to establish under ideal circumstances the qMT sensitivity of B_1 inaccuracies. MRI measurements of a small set of healthy subjects will be presented: 1) a comparison double angle and simulated variable amplitude flat B_1 maps, and 2) a comparison between three B_1 mapping methods. Similar analysis will be demonstrated on a whole brain qMT data set of an RRMS patient. A rudimentary sensitivity analysis will be discussed to provide insights on the origin and extent of the B_1 -insensitivity of the pool-size ratio.

Chapter 5: (Integrated article, Technical Note, Optional) Analytical Analysis of B_1 -Sensitivity of Quantitative Magnetization Imaging

Chapter 5 may contain the *submitted* journal article presenting a thorough B_1 -sensitivity analysis of qMT using analytical equations and/or simulated data. It is noted as optional, as it may be included in Chapter 4 if requested by the reviewers. The effects of fixing qMT parameters, which is proposed by some groups, will also be explored and reported.

Chapter 6: (Integrated article, Full Paper) Optimized Acceleration of Quantitative Magnetization Transfer Parameter Mapping Using Locally Low Rank Sparsity

Chapter 6 will contain the *submitted* journal article presenting a parameter-based compressed sensing reconstruction method applied to quantitative magnetization transfer. Single slice healthy subject data will be retroactively undersampled, and each qMT measurement will be individually assessed for sensitivity to L_1 -Spirit compressed sensing artifacts, and a measurement-varying k-space sparse acquisition protocol will be developed. Locally low rank sparsity reconstruction will then be evaluated and compared to the optimal L_1 -Spirit method developed. Lastly, qMT parameter contrast in WM lesions will be compared for both method using data from one (more if available) MS patient using the completed fast 3D protocol.

Chapter 7: Conclusion

The final chapter will summarize the thesis work, and provide concise conclusions at a level understandable to non-experts. Future work made feasible due to the technical developments of the thesis will be discussed.

FIGURES

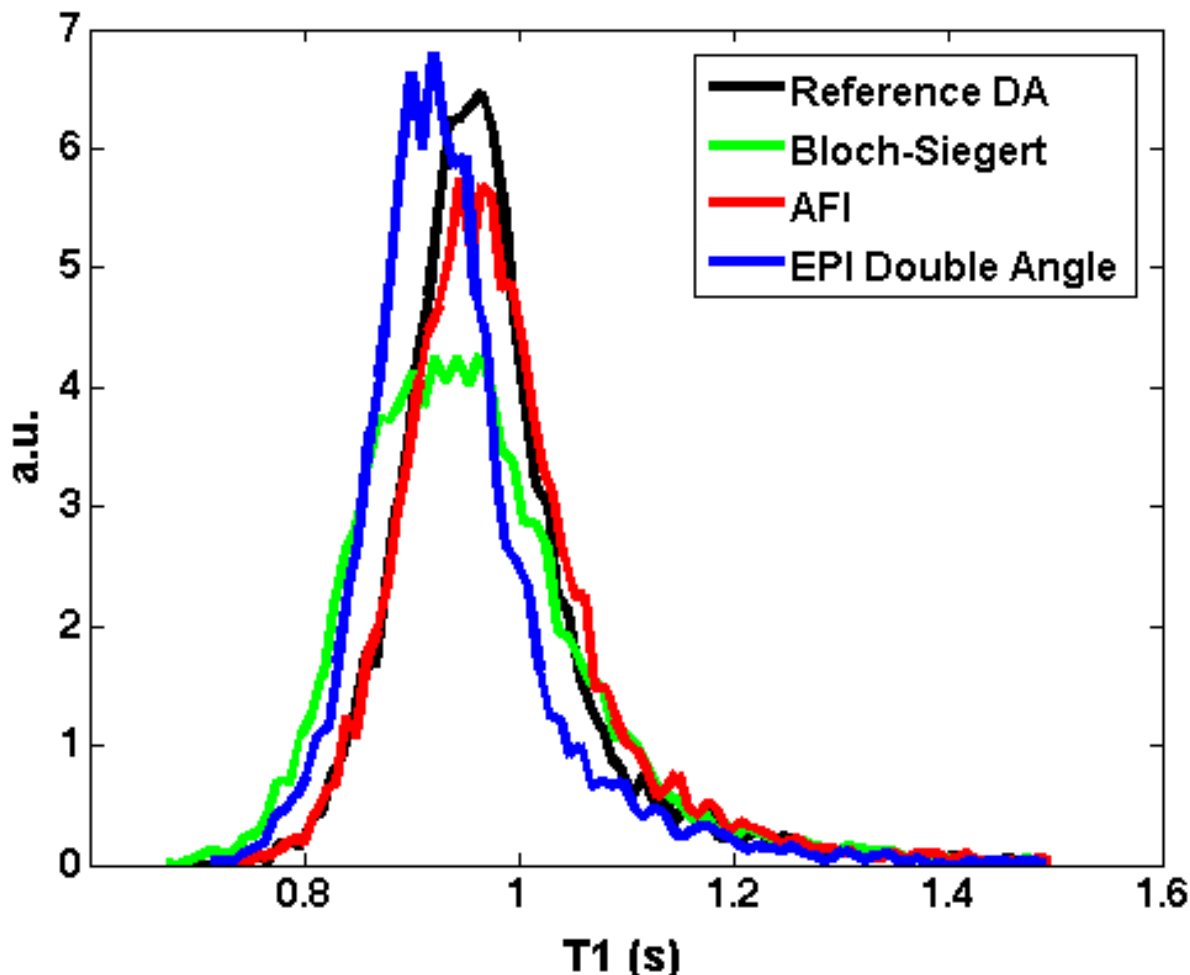


Figure 1. Normalized pooled histograms of single slice WM T_1 values for 6 healthy subjects (bin width = 10 ms).

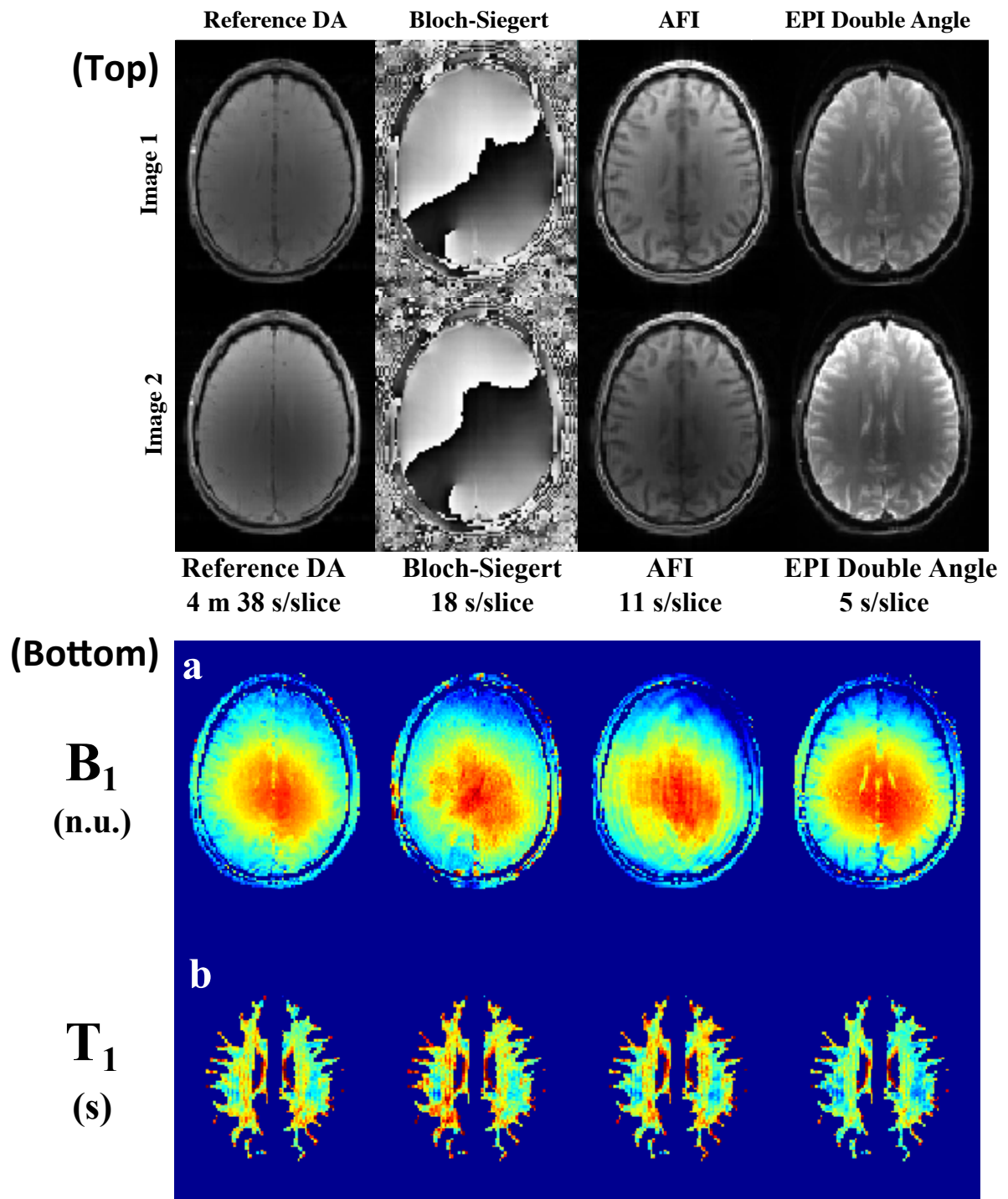


Figure 2. (Top) Raw B₁ acquisition images for each method. (Bottom) (a) Single slice B₁ maps from a representative subject. (b) WM VFA T₁ maps using flip angles corrected with each B₁ map.

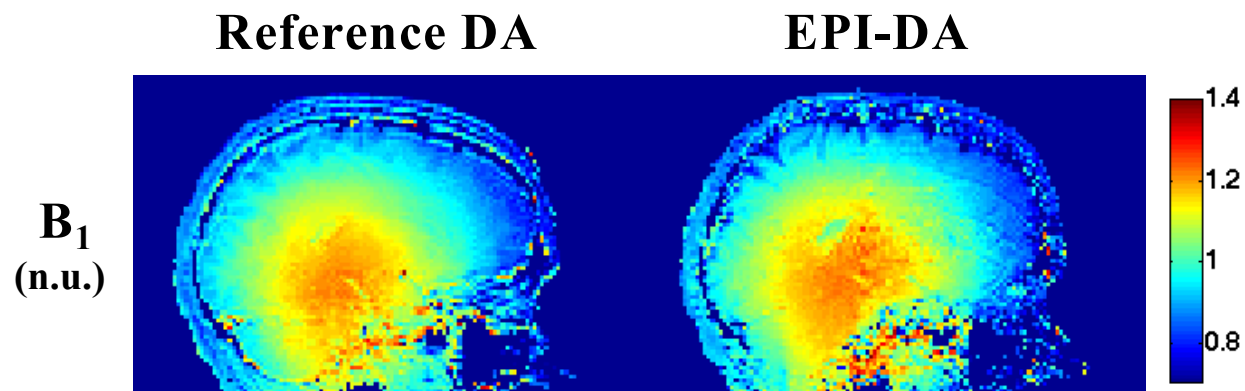


Figure 3. Sagittal (left hemisphere) B₁ maps for a single subject using the reference and EPI double angle methods.

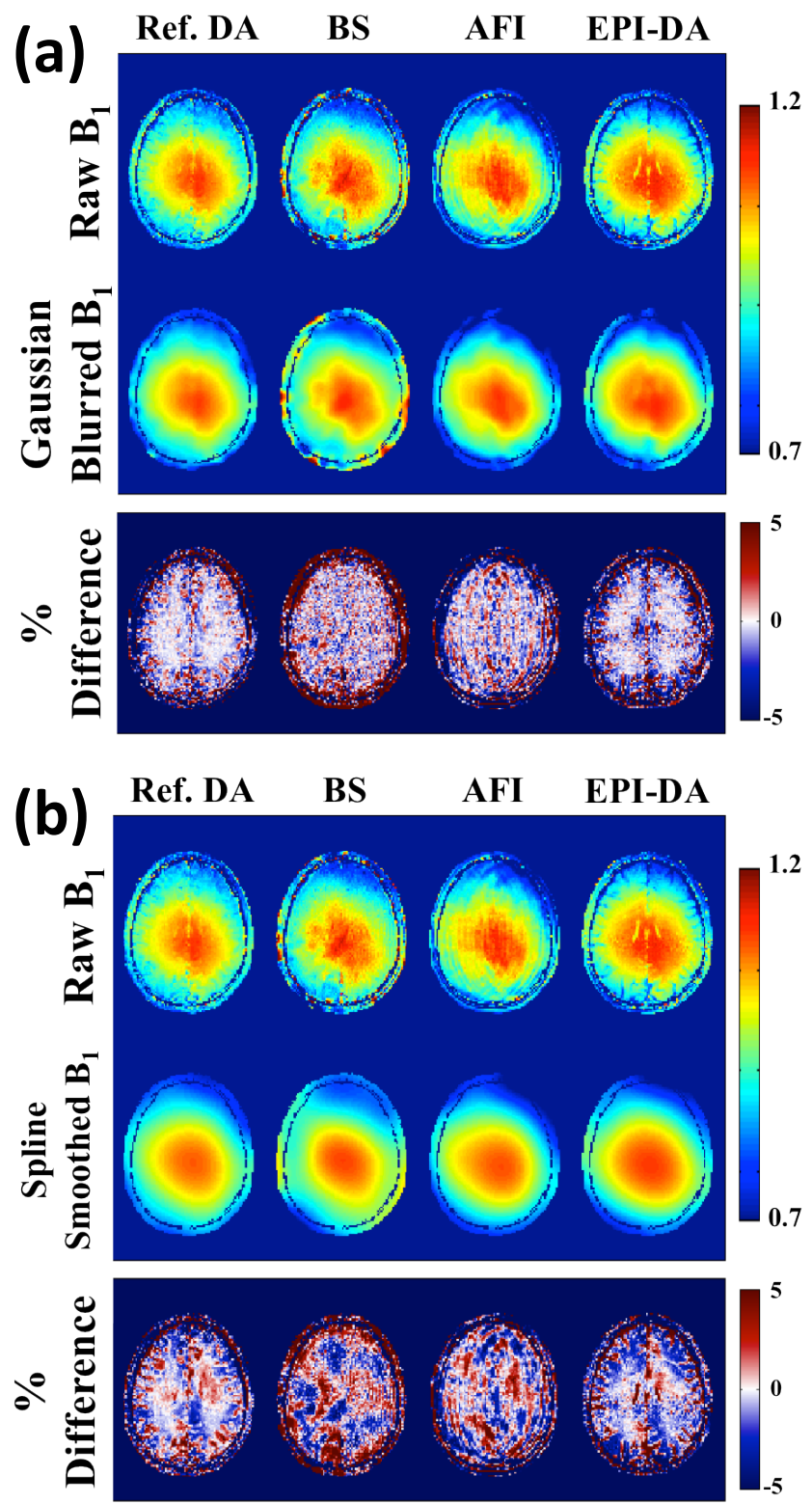


Figure 4. Comparison between raw B_1 maps and filtered maps using: **(a)** Gaussian blurring **(b)** spline smoothing.

	Ref. DA	BS	AFI	EPI-DA
Pearson ρ	-----	0.97	0.97	0.99
Fit slope	-----	0.98	1.00	0.97

Figure 5: Table listing the linear regression analysis of the pooled WM T₁ values (6 subjects) for each B₁ method relative to the reference DA B₁ method.

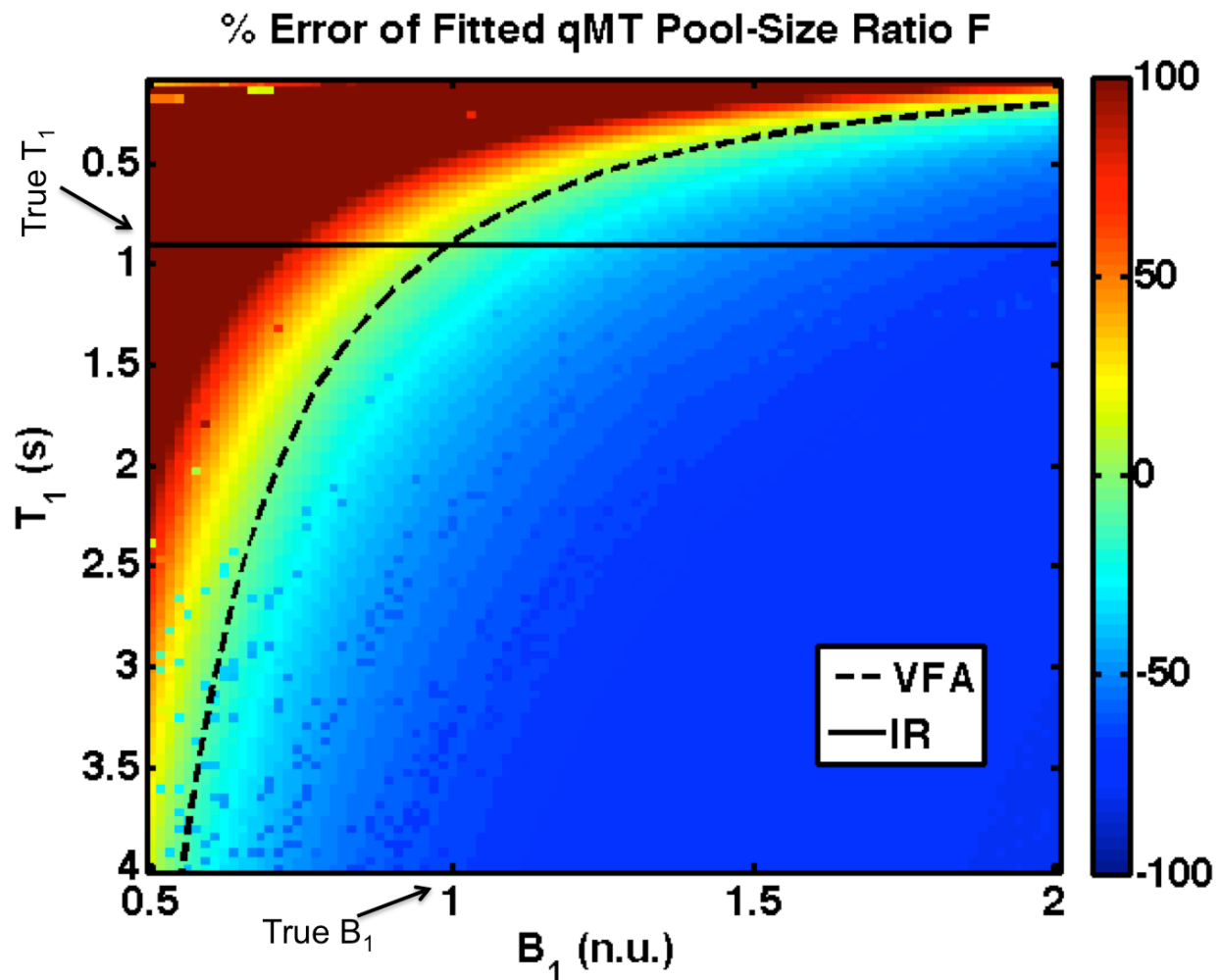


Figure 6: Percent error in fitted qMT F values in the presence of a wide range of B_1 and T_1 errors ($B_{1,\text{true}} = 1$ n.u., $T_{1,\text{true}} = 0.9$ s). The superimposed lines plot the T_1 distribution for a B_1 -independent T_1 mapping method (IR, solid line) and VFA (dashed line).

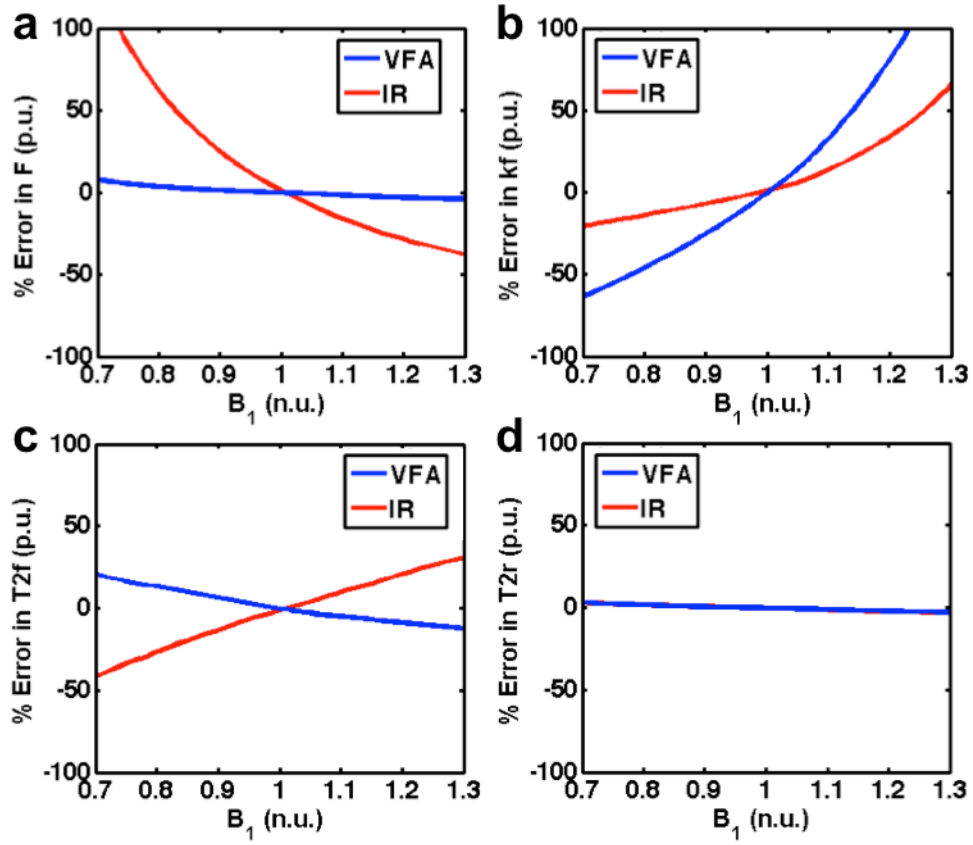


Figure 7: Percent error in fitted qMT parameters for a range of B_1 errors (**a** – pool size ratio (F), **b** – magnetization exchange rate (k_f), **c** – free pool T_2 (T_{2f}), **d** – restricted pool T_2 (T_{2r})). Fits using a B_1 -independent T_1 measure (IR) are shown in red, and those using VFA T_1 mapping are shown in blue. See solid and dashed lines in Fig. 2 for B_1 dependence of IR and VFA T_1 .

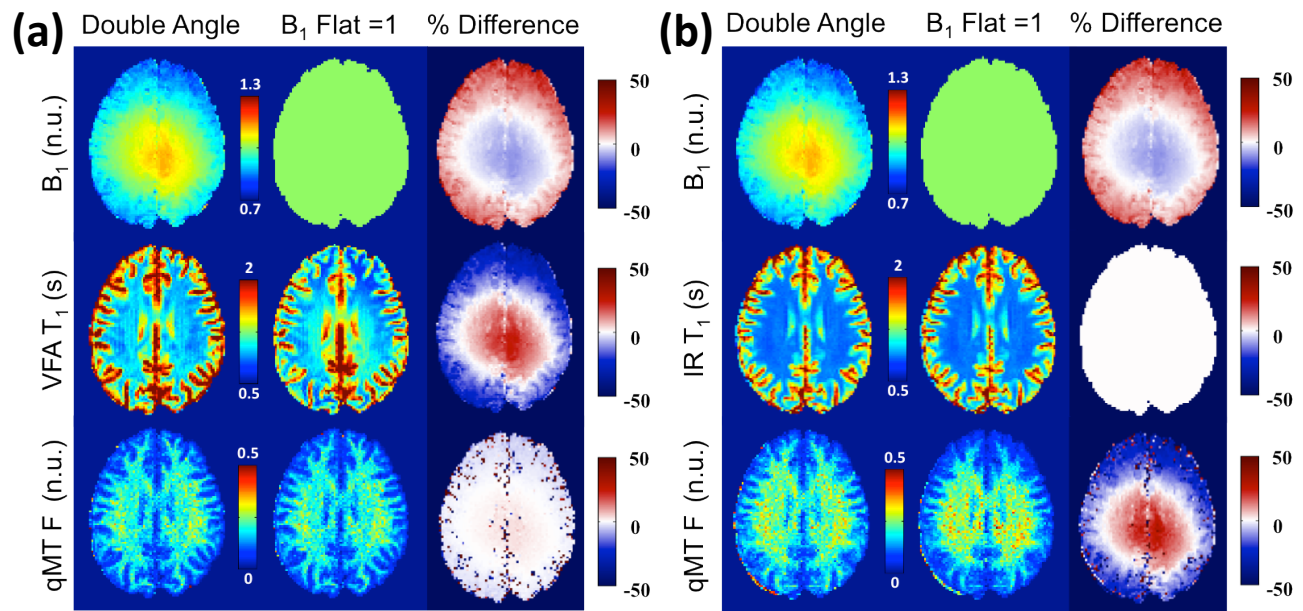


Figure 8: A single subject comparison of qMT F maps fitted using DA and flat ($B_1 = 1$) B_1 maps using (a) VFA T_1 maps corrected using the corresponding B_1 map and (b) IR T_1 maps independent of B_1 .

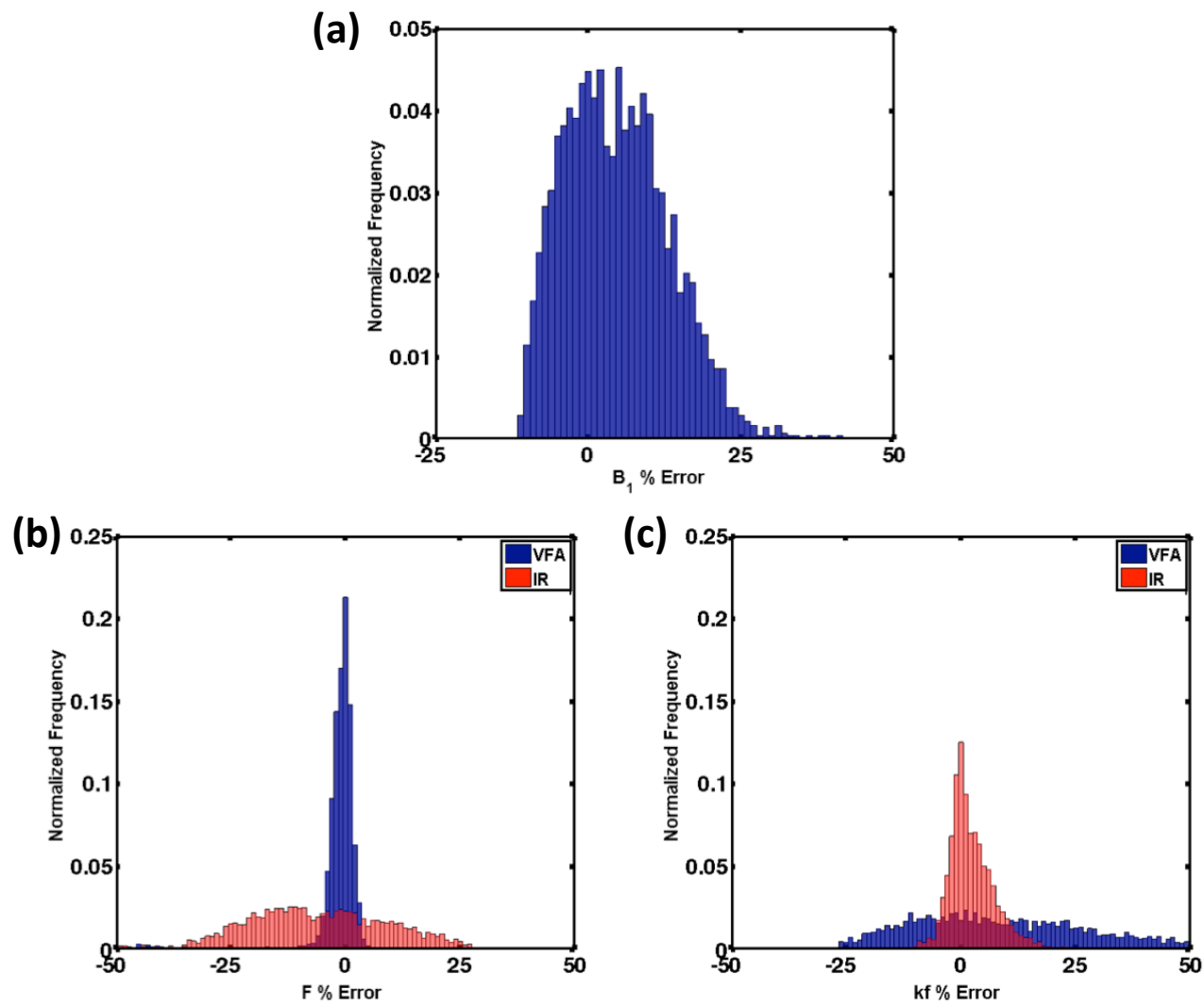


Figure 9: **a** – Histogram of B_1 error in the nominal B_1 (Flat $B_1 = 1$) assumption relative to the DA B_1 map in a single subject. **b** – Histogram of fitted qMT F error % between nominal and DA B_1 map, when using IR (red) or VFA (blue) T_1 mapping. **c** – Histogram of fitted qMT kf error % between nominal and DA B_1 map, when using IR (red) or VFA (blue) T_1 mapping.

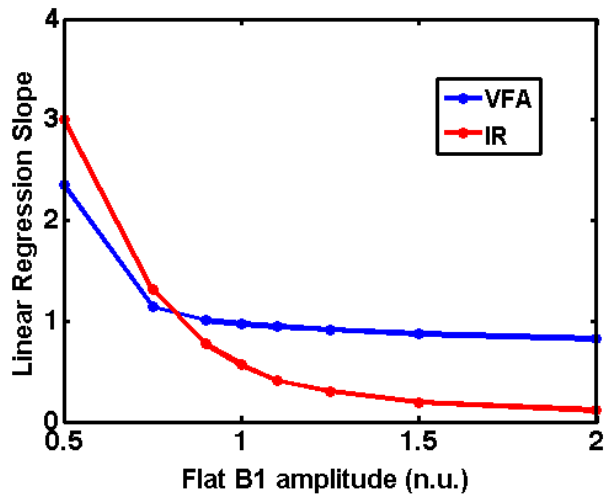
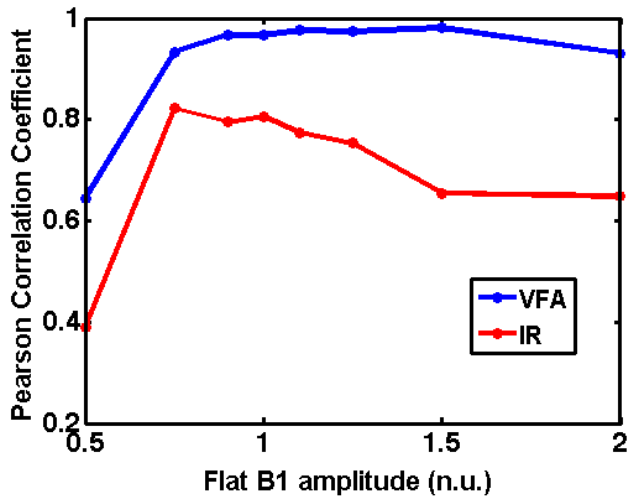
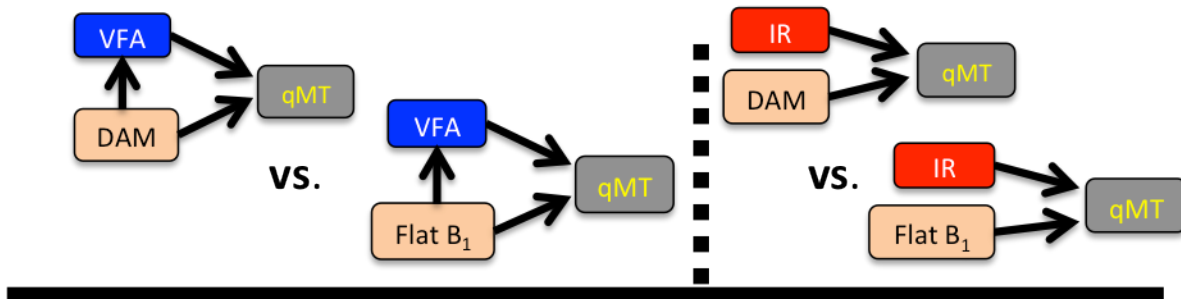


Figure 10: Pooled (all subjects) whole brain Pearson correlation coefficients (a) and linear regression slopes (b) for qMT F values between the measured DA B₁ maps and simulated flat B₁ maps.



qMT	Pearson ρ	Slope	Pearson ρ	Slope
F	0.97	0.97	0.81	0.57
k_f	0.27	0.24	0.25	0.25
R_{1f}	0.88	0.93	0.94	0.81
T_{2f}	0.98	0.86	0.93	0.90
T_{2r}	0.81	0.78	0.89	0.82

Figure 11: Pooled (all subjects) whole brain Pearson correlation coefficients and linear regression slopes for qMT F values between the measured DA B₁ maps and simulated flat B₁ maps.

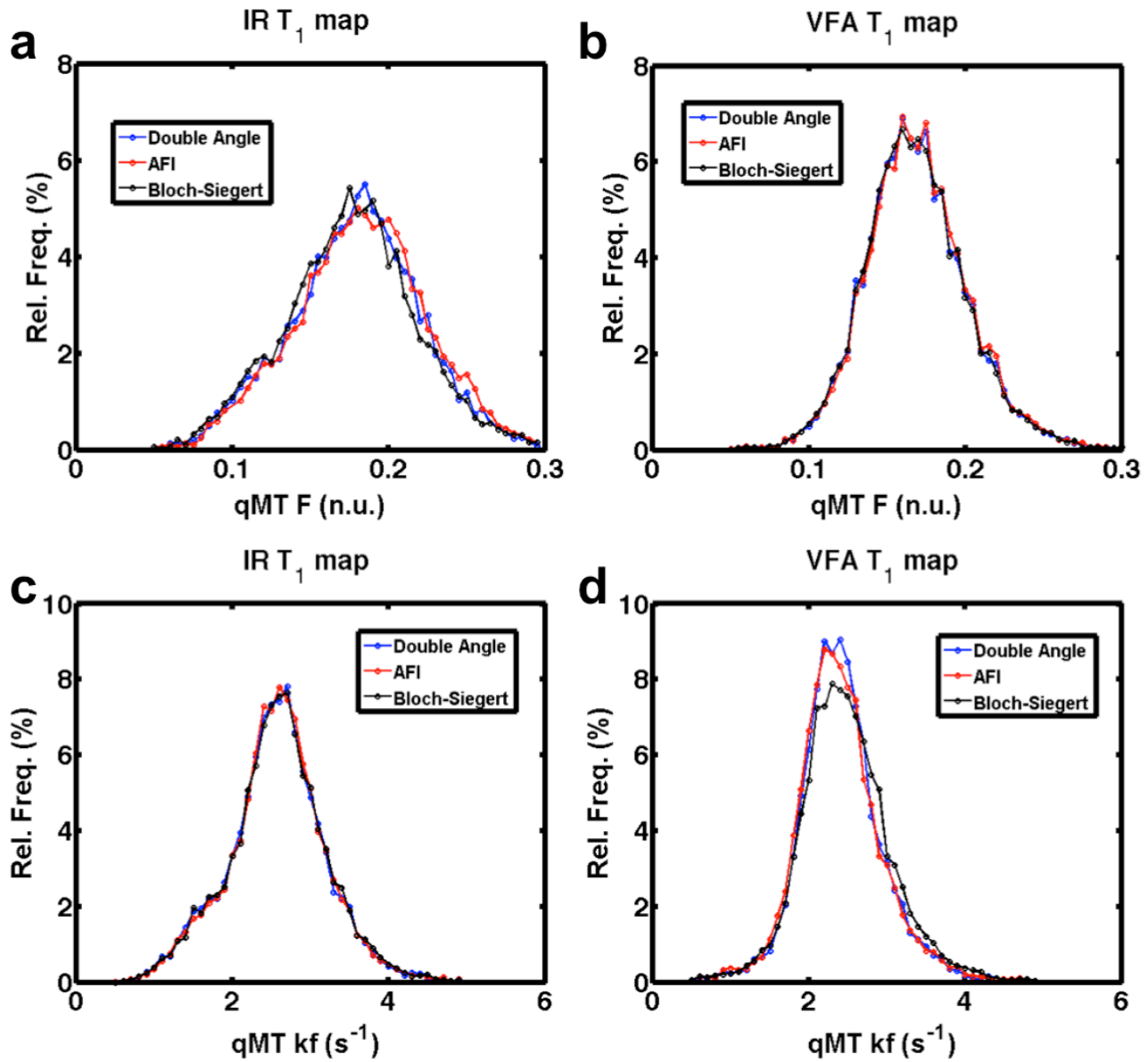


Figure 12: Single-subject WM pool-size ratio (**a, b**) and exchange coefficient (**c, d**) distributions for 3 B_1 mapping methods, using IR T_1 mapping (**a, c**) and VFA T_1 mapping (**b, d**).

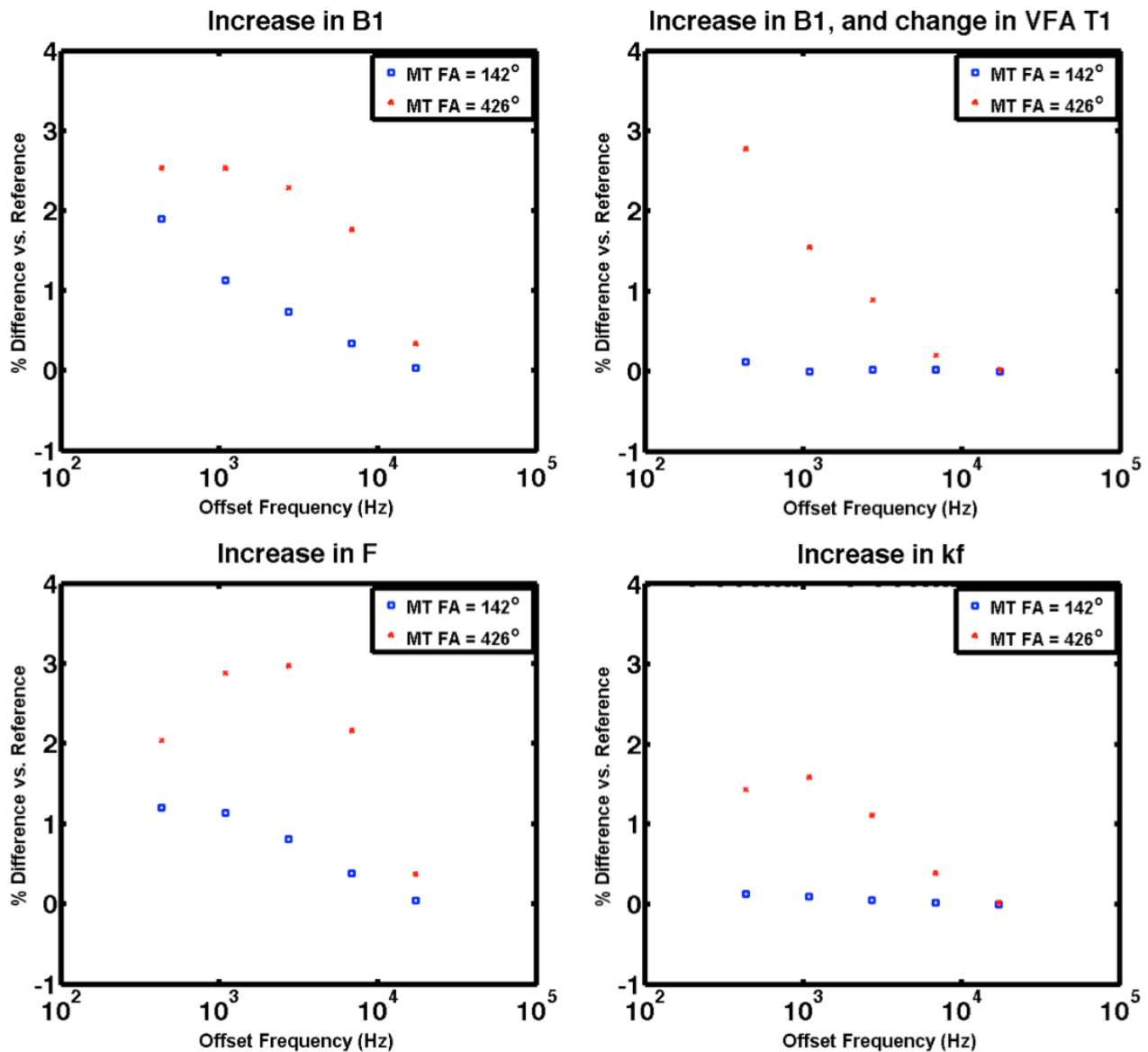


Figure 13: Sensitivity analysis of the MT signal for changes in tissue or fitting variables: **a** – 5 % increase in B_1 relative to the true B_1 , T_1 independent of B_1 **b** – 5 % increase in B_1 relative to the true B_1 , T_1 dependent of B_1 (VFA) **c** – 10% increase in the pool-size ratio F **d** – 10% increase in the MT exchange coefficient kf .

Objectives	Winter 2015	Spring 2015	Summer 2015	Fall 2015
Manuscript 1: B ₁ Method Comparison Manuscript Preparation				
Manuscript 2: B ₁ -Sensitivity Analysis of qMT RRMS Patient Data Analysis Manuscript Preparation				
Manuscript 3: Analytical qMT B ₁ -Sensitivity Analysis (optional) Analytical Analysis of B ₁ -Sensitivity Manuscript Preparation				
Manuscript 4: Accelerated 3D qMT Imaging L ₁ -SPIRiT qMT Processing Development LLR qMT Processing Development 3D qMT Data Acquisition & Analysis Manuscripts preparation		 		
Thesis Preparation				

Figure 14. Estimate timeline for the completion of the PhD thesis.

APENDIX A

Derivation of Method to Analytically Analyze Sensitivity of qMT to B_1 Inaccuracies

Let there be N measurements M_{meas} , with each measured point being approximated well by a fitted value M_{fit} dependent on L fitting or/and input variables φ :

$$\begin{bmatrix} M_{1,fit}(\varphi_1, \dots, \varphi_L) \\ \vdots \\ M_{N,fit}(\varphi_1, \dots, \varphi_L) \end{bmatrix} \cong \begin{bmatrix} M_{1,meas} \\ \vdots \\ M_{N,meas} \end{bmatrix}$$

In the case of a small error in a measured input variable $\varphi_{j,meas}$, the change in a fitted value of M_i can be approximated by a Taylor expansion:

$$M_{i,fit}(\varphi_{j,meas} + \Delta\varphi_{j,meas}) = M_{i,fit}(\varphi_j, meas) + \sum_{k=1}^L \frac{\partial M_{i,fit}}{\partial \varphi_k} \Delta\varphi_k + \dots$$

As we always fit the model to the original fitted measurement values, and we assume a good fit:

$$M_{i,fit}(\varphi_{j,meas} + \Delta\varphi_{j,meas}) \cong M_{i,meas} \equiv M_i$$

and

$$M_{i,fit}(\varphi_{j,meas}) \cong M_{i,meas} \equiv M_i$$

such that

$$M_i \cong M_i + \sum_{k=1}^L \frac{\partial M_i}{\partial \varphi_k} \Delta\varphi_k$$

Thus, any error caused by $\Delta\varphi_{j,meas}$ is compensated by variations in the other fitted parameters $\Delta\varphi_k$:

$$\sum_{\substack{k=1 \\ k \neq j}}^L \frac{\partial M_i}{\partial \varphi_k} \Delta\varphi_k + \frac{\partial M_i}{\partial \varphi_{j,meas}} \Delta\varphi_{j,meas} = 0$$

$$\sum_{\substack{k=1 \\ k \neq j}}^L \frac{\partial M_i}{\partial \varphi_k} \Delta\varphi_k = -\frac{\partial M_i}{\partial \varphi_{j,meas}} \Delta\varphi_{j,meas}$$

For qMT, the measurement we are interested in as a possible source of error is B_1 , and the fitted parameters are F, kf, T2f and T2r ($T_{1,f}$ is omitted, it's simply a function of $T_{1,meas}$, F, and kf)

$$\frac{\partial M_i}{\partial F} \Delta F + \frac{\partial M_i}{\partial k_f} \Delta k_f + \frac{\partial M_i}{\partial T_{2,f}} \Delta T_{2,f} + \frac{\partial M_i}{\partial T_{2,r}} \Delta T_{2,r} = -\frac{\partial M_i}{\partial B_1} \Delta B_1$$

The sensitivity function is defined as:

$$S_{\varphi_k, i} \equiv \frac{\partial M_i}{\partial \varphi_k}$$

Such that the previous equation can be writing compactly as:

$$\begin{bmatrix} S_{F,i} & S_{k_f,i} & S_{T_{2,f},i} & S_{T_{2,r},i} \end{bmatrix} \begin{bmatrix} \Delta F \\ \Delta k_f \\ \Delta T_{2,f} \\ \Delta T_{2,r} \end{bmatrix} = -S_{B_1,i} \Delta B_1$$

From this equation, we can provide the following general observations:

1. The larger the sensitivity functions $S_{\varphi_k,i}$, the less variation $\Delta\varphi_k$ (e.g. $\Delta F, \Delta k_f, \dots$) is required for φ_k (e.g. F, k_f, \dots) to compensate the error caused by $\Delta\varphi_{j,\text{meas}}$ (e.g. ΔB_1).
2. The smaller the sensitivity function for the measurement $S_{\varphi_k,i}$ (e.g. $S_{B_1,i} = \frac{\partial M_i}{\partial B_1}$), the less overall compensation is required by all the φ_k (e.g. F, k_f, \dots).
3. $S_{B_1,i}$ will depend on the T_1 mapping method (e.g. $S_{B_1,i}^{\text{VFA}}, S_{B_1,i}^{\text{IR}}$), due to the B_1 dependence of VFA and B_1 independence of IR T_1 maps.

For a set of N measurements (for our qMT protocols, $N=10$), this equation expands to:

$$\begin{bmatrix} S_{F,1} & S_{k_f,1} & S_{T_{2,f},1} & S_{T_{2,r},1} \\ \vdots & \vdots & \vdots & \vdots \\ S_{F,N} & S_{k_f,N} & S_{T_{2,f},N} & S_{T_{2,r},N} \end{bmatrix} \begin{bmatrix} \Delta F \\ \Delta k_f \\ \Delta T_{2,f} \\ \Delta T_{2,r} \end{bmatrix} = \begin{bmatrix} -S_{B_1,1} \Delta B_1 \\ \vdots \\ -S_{B_1,N} \Delta B_1 \end{bmatrix}$$

Which can be written in matrix form:

$$S\psi = \Psi$$

where S is the matrix of sensitivity functions, ψ is the vector of changes in fitted parameters, and Ψ is the vector of $-S_{B_1,i} \Delta B_1$.

As the equation is an overdetermined set of linear equations of the form:

$$Ax = b$$

The optimal changes in parameters ψ can be solved through the following minimization:

$$\min \|S\psi - \Psi\|_2^2$$

for different protocols, B_1 mapping methods, etc. S and Ψ can be calculated analytically (possible, but cumbersome to do so), or estimated through simulations.

From this analysis, and from my qMT B1-insensitivity measurements, we can make the following general predictions:

- $|S_{F,i}| \gg |S_{k_f,i}|$ for most measurements when using VFA, since we expect $\Delta F \cong 0$
- $|S_{k_f,i}| \ll |S_{F,i}|, |S_{T_{2,f},i}|, |S_{T_{2,r},i}|$ for most measurements when using VFA (most of the error is dumped into kf)
- $|S_{B_1,i}^{VFA}| < |S_{B_1,i}^{IR}|$ since less ΔF is required for VFA and IR. (This one is less strong, since Δk_f is smaller for IR and VFA, but for ΔF it's the opposite. Possibly a more complicated relationship to the solution of minimization instead of this simple relation)

APENDIX B

**2015 ISMRM Conference Abstract – 1
(Submitted, First author)**

B₁-Sensitivity Analysis of qMTMathieu Boudreau¹, Nikola Stikov¹, and G. Bruce Pike²¹McConnell Brain Imaging Center, Montreal Neurological Institute, McGill University, Montreal, Quebec, Canada, ²Hotchkiss Brain Institute, Faculty of Medicine, University of Calgary, Calgary, Alberta, Canada

INTRODUCTION: B₁ mapping is an important measurement used in quantitative magnetization transfer (qMT) imaging, particularly at high field strengths (≥ 3.0 T) where B₁ can vary by $\pm 30\%$ in a human brain (Fig. 1). For pulsed spoiled gradient echo (SPGR) qMT imaging experiments, B₁ maps are used as a corrective factor for the excitation flip angle (-5° to 15°) and MT saturation power (flip angles ~150° to 700°). Additional measurements necessary for qMT (e.g. T₁ mapping) may also require B₁ maps as a corrective factor; variable flip angle (VFA) T₁ mapping requires B₁ maps, while inversion recovery (IR) or Look-Locker typically do not¹. Thus, local (e.g. artifacts) or global (e.g. systemic biases) inaccuracies in B₁ mapping² will propagate to the fitted qMT parameters differently, depending on the chosen T₁ mapping method.

We recently reported that the qMT pool-size ratio (F), an important myelin biomarker, is insensitive to a large range of B₁ inaccuracies when using VFA for T₁ mapping³ (Fig. 1). Here we present a simulation-based analysis of the B₁ sensitivity of qMT, comparing how different T₁ mapping methods (VFA vs. IR) propagate the B₁ error to the qMT parameters. We show that the F parameter is very robust and insensitive to B₁ inaccuracies when VFA T₁ mapping is used, but this comes at the expense of a substantial increase in error of kf.

METHODS: The Bloch-McConnell equations for magnetization exchange were solved using MATLAB (MATLAB2011a, The Mathworks Inc.) for a pulsed SPGR experiment by decomposing the pulse sequence into periods of instantaneous saturation of the free pool, constant irradiation of the restricted pool, and free precession⁴. Healthy white matter tissue parameters were fixed to the following values: F = 0.122, kf = 3.97 s⁻¹, R1f = 1.11 s⁻¹, R1r = 1.0 s⁻¹, T2f = 27.2 ms, T2r = 10.96 μs. The MT signal was simulated from the solution of the Bloch-McConnell equation for the following MT protocol: TR = 25 ms, $\alpha_{\text{excitation}} = 7^\circ$, Gaussian-Hanning MT pulses with a pulse duration of 10.2 ms, $\alpha_{\text{MT}} = 142^\circ$ and 426°, logarithmically spaced off-resonance frequencies = 423.9 Hz, 1,087.5 Hz, 2,731.6 Hz, 6,861.6 Hz, and 17,235.4 Hz. The MT signal was subsequently fitted using the Sled and Pike method⁵ for a linear range of 100 B₁ and 100 T₁ values (10,000 points in total); T₁ varied independently of B₁ for this step, and without any assumptions on the measurement method. B₁ ranged from 0.5 to 2 (B_{1,true} = 1), and T₁ ranged from 0.1 s to 4 s (T_{1,true} = 0.9 s). VFA signals were also simulated from the analytical SPGR equation¹. TR = 25 ms, $\alpha = 3^\circ$ and 20°, T₁ = T_{1,true}. T₁ values were fitted from the VFA data for the B₁ error range. The fitted T₁ values were subsequently used in conjunction with their respective B₁ values to fit the MT signal.

RESULTS: Figure 2 shows the error (%) of the fitted qMT pool-size ratio, F, in the presence of a wide range of B₁ and T₁ inaccuracies (B_{1,true} = 1, T_{1,true} = 0.9 s). The superimposed lines show the range of errors expected from an experiment using a B₁-independent T₁ method like IR (solid line), and from VFA T₁ mapping (dashed line). Figure 3 plots the errors in qMT fitted parameters (F, kf, T_{2f}, T_{2r}) using B₁-independent (IR) and VFA measured T₁ (see lines in Fig. 2), for a range of B₁ inaccuracies typically observed in vivo. Errors in F induced by B₁ errors were greatly reduced using VFA T₁ mapping (Fig. 3a). A substantial increase in errors in kf occurs for VFA relative to IR (Fig. 3b), while T_{2r} remains insensitive to B₁ inaccuracies for both cases.

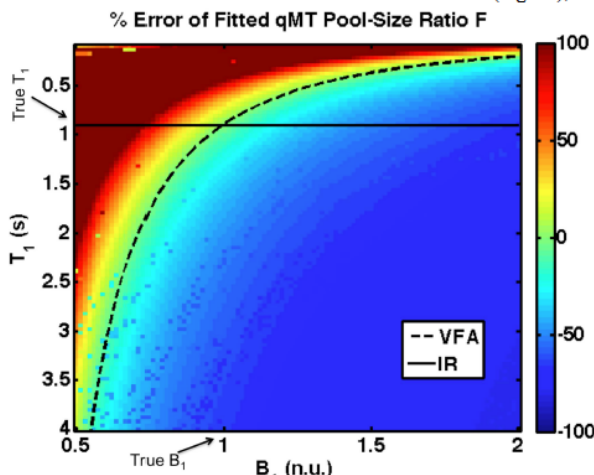


Figure 2. Percent error in fitted qMT F values in the presence of a wide range of B₁ and T₁ errors (B_{1,true} = 1 n.u., T_{1,true} = 0.9 s). The superimposed lines plot the T₁ distribution for a B₁-independent T₁ mapping method (IR, solid line) and VFA (dashed line).

DISCUSSION: The qMT pool size ratio F was shown to be nearly B₁-error insensitive when using VFA T₁ mapping (Fig. 3a - blue). Using a B₁-independent T₁ measure such as IR produces large qMT F errors (from >100% to -45% for B₁ errors ranging from -30% to 30%, Fig 3a - red), while VFA T₁ mapping kept qMT F errors within a moderate range (7% to -3%, Fig. 3a - blue). The B₁ errors for the case of VFA were mostly absorbed by the kf parameters (Fig. 3b), in agreement with observations from previous *in vivo* work³. These results suggest that qMT imaging using B₁-independent T₁ measurement, and qMT methods that fixes qMT model parameters, may have increased sensitivity to B₁-inaccuracies. However, for applications where kf may be the biomarker of interest (e.g. cartilage imaging⁶, systemic inflammation⁷), a B₁-independent measure of T₁ may be preferred instead of the VFA method. Further analytical sensitivity analysis of the qMT equations for different qMT measurement protocols could help determine optimal qMT protocols for reduced B₁-inaccuracy sensitivity.

REFERENCES: [1] Stikov, N. et al., MRM, doi: 10.1002/mrm.25135 (2014) [2] Boudreau, M. et al., Proc. of ISMRM, #3207 (2014) [3] Boudreau, M. et al., Proc. of ISMRM, #3167 (2014) [4] Sled J. and Pike G. B., JMR, 145:24-36 (2000) [5] Sled J. and Pike G. B., MRM, 46:923-931 (2001) [6] Stikov, N. et al., MRM, 66:725-734 (2011) [7] Harrison, N. et al., Biological Psychiatry, DOI: 10.1016/j.biopsych.2014.09.023 (2014)

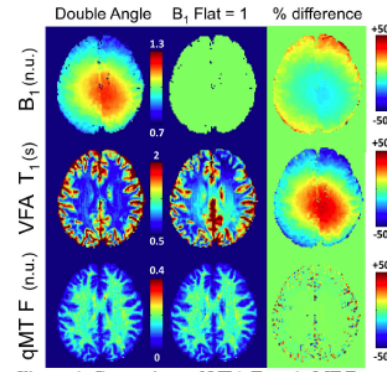


Figure 1. Comparison of VFA T₁ and qMT F maps using measured and nominal (B₁ flat = 1) B₁ maps at 37°.

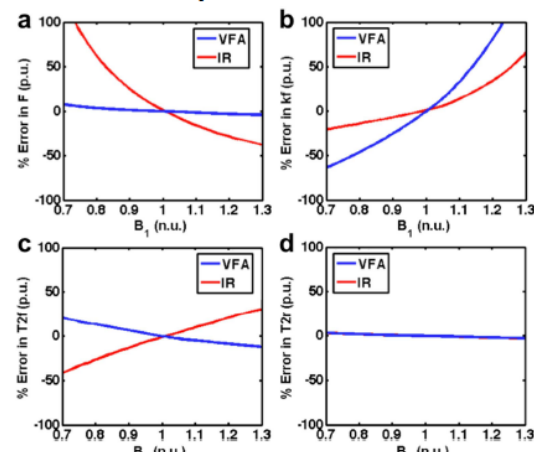


Figure 3. Percent error in fitted qMT parameters for a range of B₁ errors (a – pool size ratio (F), b – magnetization exchange rate (kf), c – free pool T_{2f}, d – restricted pool T₂ (T_{2r})). Fits using a B₁-independent T₁ measure (IR) are shown in red, and those using VFA T₁ mapping are shown in blue. See solid and dashed lines in Fig. 2 for B₁ dependence of IR and VFA T₁.

APENDIX C

**2015 ISMRM Conference Abstract – 2
(Submitted, coauthor)**

Quantitative Magnetization Transfer Analysis: An Interactive Introduction with qMTLab

Ye Gu¹, Mathieu Boudreau², Ives R. Levesque³, Yaaseen Atchia⁴, John G. Sled^{5,6}, Sridar Narayanan², Douglas L. Arnold³, Bruce Pike^{2,7}, and Nikola Stikov^{8,9}
¹NeuroRx Research, Montreal, QC, Canada, ²Montreal Neurological Institute, McGill University, Montreal, QC, Canada, ³Medical Physics, Oncology and RI-MUHC, McGill University, Montreal, QC, Canada, ⁴Electrical and Biomedical Engineering, University of Toronto, Toronto, ON, Canada, ⁵Hospital for Sick Children, Toronto, ON, Canada, ⁶Medical Biophysics, University of Toronto, Toronto, ON, Canada, ⁷Radiology, University of Calgary, Calgary, AB, Canada, ⁸Montreal Heart Institute, Montreal, QC, Canada, ⁹Institute for Biomedical Engineering, Ecole Polytechnique, Montreal, QC, Canada

PURPOSE: Magnetization transfer (MT) imaging is an important tool in the study of the macromolecular content of tissue¹. It is well-established that quantitative MT (qMT) offers improved specificity to myelin content, leading to a better understanding of pathology in demyelinating diseases such as MS^{2,3,4,5}. Recent studies have also extended the application of qMT to studying articular cartilage⁶ and cancer⁷. A wide range of qMT techniques are available, and they can generally be grouped in two broad categories: on- and off-resonance^{8,9}. Because of the differences in terminology and pulse sequence implementation, it is difficult to provide a unified framework for qMT data processing and analysis. In this abstract, a user-friendly, GUI-based software package is described that explains the basics of qMT and includes functionalities for simulation, sensitivity testing, and fitting of a number of qMT protocols. The package, named qMTLab, will be made available to the public, with the intention to become an open-source analysis tool for qMT researchers and users.

OUTLINE OF CONTENT: A GUI based software package was built, using the GUIDE development platform in MATLAB (The MathWorks, Natick USA), for the purpose of simulation, sensitivity testing, fitting, and processing of qMT data. All processing and fitting algorithms – including a standard least-square fitting for the *on-resonance* bSSFP model and a rectangular pulse approximation method for the *off-resonance* SPGR model – were also developed in MATLAB and are capable of handling the DICOM and MINC file formats. The design concepts were: 1) to develop the entire package in separate modules for different functions (simulation, sensitivity analysis, data handling, processing); 2) to ensure compatibility between modules so that data is easily saved/loaded across modules; and 3) to make the package open-source and design the data structure to allow users to easily customize qMT protocols and add-ons.

Figure 1 shows one screenshot of the qMTLab interface, focusing on the single-voxel data-fitting module of the package. This module allows users to visualize the behavior of the fitting routine based on the choice of data points and acquisition parameters. Users can fix certain parameters while varying others (red arrow labeled A), to perform a quick sensitivity analysis. This module also allows user-generated protocols to be pre-saved, and to select the data points used in the fit (blue arrow labeled B), resulting in a flexible and customizable package. Separate on- and off-resonance modules enable simulation of qMT data sets, and customized data fitting (not shown here). The detailed function of each module is listed in Table 1.

Table 1: Description of the functionality of each module of qMTLab

Module	Functionality
Bloch equation simulator	Uses a two-pool model and Bloch equations with cross-relaxation terms and arbitrarily shaped RF pulses. Simulates the bSSFP (<i>on-resonance</i>) and SPGR (<i>off-resonance</i>) sequences numerically using the MATLAB differential equation solver
Analytical model viewer	Visualizes the behavior of the analytical model by varying the qMT parameters. Visualizes the effectiveness of the multi-pulse approximation for a given shaped <i>off-resonance</i> MT pulse.
Single-voxel fitting and sensitivity analysis	Characterize the sensitivity of the fitting to each qMT parameter. Compute and visualize absorption rates and direct effect of customized off-resonance pulse shape.
Processing interface	Fit real data for existing qMT protocols using an arbitrary range of flip-angles and TRs. Allow the implementation of custom qMT protocols.

SUMMARY: qMTLab allows easy visualization and manipulation of qMT data, making it possible to evaluate and compare various qMT protocols. The two main advantages of qMTLab are its modular design and its compatibility with extensions and customizations. qMTLab also provides a framework for standardizing the validation and fitting of qMT data. The software package is developed and will be made freely available¹⁰ to the MR community. We hope it will become a valuable tool for future qMT studies, leading the way toward fast, robust and clinically feasible qMT protocols.

REFERENCES: [1] Wolff and Balaban. Magn. Reson. Med. 10(1):135-144, (1989). [2] Garcia *et al.* Neuroimage 52(2): 532-537, (2010). [3] Schmieder *et al.* J. Magn. Reson. Imaging, 26: 41–51, (2007). [4] Ropele *et al.* American J Neurol: 1-10 (2012). [5] Levesque *et al.* Magn. Reson. Med., 63: 633-640, (2010). [6] Stikov *et al.* Magn. Reson. Med. 66:725-734, (2011). [7] Underhill *et al.* Neuroimage 54(3): 2052-2065 (2010). [8] Sled and Pike. J. Magn. Res. 145(1): 24-36, (2001). [9] Gloor *et al.* Magn. Reson. Med. 45: 265-269 (2008). [10] <https://github.com/sharktank-bic/qMTLab>

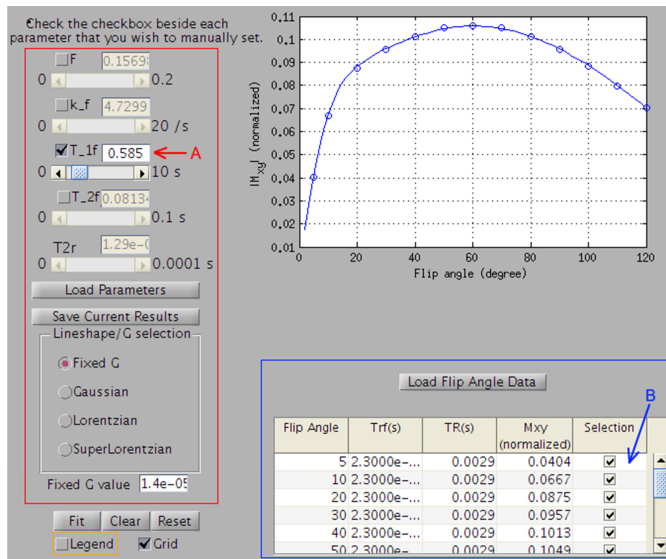


Figure 1: Screenshot of the qMTLab fitting routine. The red square shows the parameter setting area. The blue square shows the data loading and selection area

APENDIX D

**In vivo histology of the myelin g-ratio with magnetic resonance imaging - Neuroimage
(Submitted, coauthor)**

***7. Manuscript**

[Click here to view linked References](#)

In vivo histology of the myelin g-ratio with magnetic resonance imaging

Nikola Stikov^{a,d*}, Jennifer S.W. Campbell^{a*}, Thomas Stroh^a, Stephen Frey^a, Jennifer Novek^a,
Stephen Nuara^a, Ming-Kai Ho^a, Barry J. Bedell^a, Robert
F. Dougherty^b, Ilana R. Leppert^a, Mathieu Boudreau^a, Sridar Narayanan^{a,c},
and G. Bruce Pike^a

^a*Montreal Neurological Institute, McGill University, Montreal, Canada*

^b*Stanford University, Stanford, California, United States*

^c*Hotchkiss Brain Institute and Department of Radiology,
University of Calgary, Calgary, Alberta, Canada*

^d*École Polytechnique de Montréal, Montréal, Canada*

*these authors contributed equally to this work

Corresponding author:

Nikola Stikov
Institute of Biomedical Engineering
École Polytechnique de Montréal
2900 Edouard-Montpetit Bld, room L-5610
Montreal, QC
H3T 1J4
phone: 514-340-5121

Abstract

The myelin g-ratio, defined as the ratio between the inner and the outer diameter of the myelin sheath, is a fundamental property of white matter that can be computed from a simple formula relating the myelin volume fraction to the fiber volume fraction or the axon volume fraction. In this paper, a unique combination of magnetization transfer, diffusion imaging and histology is presented, providing a novel method for computing the axon volume fraction and for validating the *in vivo* magnetic resonance imaging measurements of the myelin g-ratio. Our method was validated in the corpus callosum of one cynomolgus macaque, and applied to obtain full-brain g-ratio maps in one healthy human subject and one multiple sclerosis patient. In the macaque, the g-ratio computed from MRI correlated well with the g-ratio from histology ($r = 0.82$, $p = 0.01$). In the human subjects, the g-ratio in multiple sclerosis lesions was higher than in normal appearing white matter, which was in turn higher than in healthy white matter. Measuring the g-ratio brings us one step closer to fully characterizing white matter non-invasively, making it possible to perform *in vivo* histology of the human brain during development, aging, disease and treatment.

Keywords

myelin g-ratio, magnetization transfer, quantitative MRI, diffusion, histology, white matter microstructure

References

1. MSSC. <http://www.mssociety.ca/en/information>. MS Society of Canada 2012.
2. Polman CH, Reingold SC, Banwell B, Clanet M, Cohen JA, Filippi M, Fujihara K, Havrdova E, Hutchinson M, Kappos L, Lublin FD, Montalban X, O'Connor P, Sandberg-Wollheim M, Thompson AJ, Waubant E, Weinshenker B, Wolinsky JS. Diagnostic criteria for multiple sclerosis: 2010 revisions to the McDonald criteria. *Ann Neurol* 2011;69(2):292-302.
3. Frohman EM, Racke MK, Raine CS. Multiple sclerosis--the plaque and its pathogenesis. *The New England journal of medicine* 2006;354(9):942-955.
4. McFarland HF, Martin R. Multiple sclerosis: a complicated picture of autoimmunity. *Nature immunology* 2007;8(9):913-919.
5. Noseworthy JH, Lucchinetti C, Rodriguez M, Weinshenker BG. Multiple sclerosis. *The New England journal of medicine* 2000;343(13):938-952.
6. Peterson JW, Bo L, Mork S, Chang A, Trapp BD. Transected neurites, apoptotic neurons, and reduced inflammation in cortical multiple sclerosis lesions. *Ann Neurol* 2001;50(3):389-400.
7. Schmierer K, Thavarajah JR, An SF, Brandner S, Miller DH, Tozer DJ. Effects of formalin fixation on magnetic resonance indices in multiple sclerosis cortical gray matter. *Journal of magnetic resonance imaging : JMRI* 2010;32(5):1054-1060.
8. Stadelmann C, Albert M, Wegner C, Bruck W. Cortical pathology in multiple sclerosis. *Current opinion in neurology* 2008;21(3):229-234.
9. Perry VH, Anthony DC. Axon damage and repair in multiple sclerosis. *Philosophical transactions of the Royal Society of London Series B, Biological sciences* 1999;354(1390):1641-1647.
10. Lassmann H. Axonal and neuronal pathology in multiple sclerosis: What have we learnt from animal models. *Experimental neurology* 2010;225(1):2-8.
11. Staigaitis SM, Chang A, Trapp BD. Cortical pathology in multiple sclerosis: experimental approaches to studies on the mechanisms of demyelination and remyelination. *Acta Neurologica Scandinavica* 2012;126:97-102.
12. Klaver R, De Vries HE, Schenk GJ, Geurts JJ. Grey matter damage in multiple sclerosis: A pathology perspective. *Prion* 2013;7(1).
13. Brownell B, Hughes JT. The distribution of plaques in the cerebrum in multiple sclerosis. *Journal of neurology, neurosurgery, and psychiatry* 1962;25:315-320.
14. Calabrese M, Agosta F, Rinaldi F, Mattisi I, Grossi P, Favaretto A, Atzori M, Bernardi V, Barachino L, Rinaldi L, Perini P, Gallo P, Filippi M. Cortical Lesions and Atrophy Associated With Cognitive Impairment in Relapsing-Remitting Multiple Sclerosis. *Archives of neurology* 2009;66(9):1144-1150.
15. Simon JH, Li D, Traboulsee A, Coyle PK, Arnold DL, Barkhof F, Frank JA, Grossman R, Paty DW, Radue EW, Wolinsky JS. Standardized MR imaging protocol for multiple sclerosis: Consortium of MS Centers consensus guidelines. *AJNR American journal of neuroradiology* 2006;27(2):455-461.
16. Schmierer K, Scaravilli F, Altmann DR, Barker GJ, Miller DH. Magnetization transfer ratio and myelin in postmortem multiple sclerosis brain. *Ann Neurol* 2004;56(3):407-415.
17. Schmierer K, Tozer DJ, Scaravilli F, Altmann DR, Barker GJ, Tofts PS, Miller DH. Quantitative magnetization transfer imaging in postmortem multiple sclerosis brain. *Journal of magnetic resonance imaging : JMRI* 2007;26(1):41-51.

18. Levesque I, Sled JG, Narayanan S, Santos AC, Brass SD, Francis SJ, Arnold DL, Pike GB. The role of edema and demyelination in chronic T-1 black holes: A quantitative magnetization transfer study. *Journal of Magnetic Resonance Imaging* 2005;21(2):103-110.
19. Levesque IR, Giacomini PS, Narayanan S, Ribeiro LT, Sled JG, Arnold DL, Pike GB. Quantitative magnetization transfer and myelin water imaging of the evolution of acute multiple sclerosis lesions. *Magnetic resonance in medicine : official journal of the Society of Magnetic Resonance in Medicine / Society of Magnetic Resonance in Medicine* 2010;63(3):633-640.
20. Tardif CL, Bedell BJ, Eskildsen SF, Collins DL, Pike GB. Quantitative Magnetic Resonance Imaging of Cortical Multiple Sclerosis Pathology. *Multiple Sclerosis International* 2012;2012:13.
21. Arnold DL, Matthews PM. MRI in the diagnosis and management of multiple sclerosis. *Neurology* 2002;58(8 suppl 4):S23-S31.
22. Anderson VM, Fox NC, Miller DH. Magnetic resonance imaging measures of brain atrophy in multiple sclerosis. *Journal of Magnetic Resonance Imaging* 2006;23(5):605-618.
23. De Stefano N, Battaglini M, Smith SM. Measuring Brain Atrophy in Multiple Sclerosis. *Journal of Neuroimaging* 2007;17:10S-15S.
24. Sepulcre J, Goni J, Masdeu JC, Bejarano B, de Mendizabal NV, Toledo JB, Villoslada P. Contribution of White Matter Lesions to Gray Matter Atrophy in Multiple Sclerosis. *Archives of neurology* 2009;66(2):173-179.
25. Derakhshan M, Caramanos Z, Giacomini PS, Narayanan S, Maranzano J, Francis SJ, Arnold DL, Collins DL. Evaluation of automated techniques for the quantification of grey matter atrophy in patients with multiple sclerosis. *NeuroImage* 2010;52(4):1261-1267.
26. Filippi M, Agosta F. Magnetic resonance techniques to quantify tissue damage, tissue repair, and functional cortical reorganization in multiple sclerosis. *Progress in brain research* 2009;175:465-482.
27. Kidd D, Barkhof F, McConnell R, Algra PR, Allen IV, Revesz T. Cortical lesions in multiple sclerosis. *Brain : a journal of neurology* 1999;122 (Pt 1):17-26.
28. Bedell BJ, Narayana PA. Implementation and evaluation of a new pulse sequence for rapid acquisition of double inversion recovery images for simultaneous suppression of white matter and CSF. *Journal of magnetic resonance imaging : JMRI* 1998;8(3):544-547.
29. Filippi M, Rocca MA. Multiple sclerosis and allied white matter diseases. *Neurological sciences : official journal of the Italian Neurological Society and of the Italian Society of Clinical Neurophysiology* 2008;29 Suppl 3:319-322.
30. Wolff SD, Balaban RS. Magnetization transfer contrast (MTC) and tissue water proton relaxation in vivo. *Magnetic resonance in medicine : official journal of the Society of Magnetic Resonance in Medicine / Society of Magnetic Resonance in Medicine* 1989;10(1):135-144.
31. Henkelman RM, Huang X, Xiang QS, Stanisz GJ, Swanson SD, Bronskill MJ. Quantitative interpretation of magnetization transfer. *Magnetic resonance in medicine : official journal of the Society of Magnetic Resonance in Medicine / Society of Magnetic Resonance in Medicine* 1993;29(6):759-766.
32. Graham SJ, Henkelman RM. Understanding pulsed magnetization transfer. *Journal of magnetic resonance imaging : JMRI* 1997;7(5):903-912.
33. Henkelman RM, Stanisz GJ, Graham SJ. Magnetization transfer in MRI: a review. *NMR in biomedicine* 2001;14(2):57-64.

34. Ge Y, Kolson DL, Babb JS, Mannon LJ, Grossman RI. Whole brain imaging of HIV-infected patients: quantitative analysis of magnetization transfer ratio histogram and fractional brain volume. *AJNR American journal of neuroradiology* 2003;24(1):82-87.
35. Dousset V, Armand JP, Huot P, Viaud B, Caille JM. Magnetization transfer imaging in AIDS-related brain diseases. *Neuroimaging clinics of North America* 1997;7(3):447-460.
36. Wu Y, Storey P, Carrillo A, Saglamer C, Cohen BA, Epstein LG, Edelman RR, Ragin AB. Whole brain and localized magnetization transfer measurements are associated with cognitive impairment in patients infected with human immunodeficiency virus. *AJNR American journal of neuroradiology* 2008;29(1):140-145.
37. Fornari E, Maeder P, Meuli R, Ghika J, Knyazeva MG. Demyelination of superficial white matter in early Alzheimer's disease: a magnetization transfer imaging study. *Neurobiology of aging* 2012;33(2):428 e427-419.
38. Giulietti G, Bozzali M, Figura V, Spano B, Perri R, Marra C, Lacidogna G, Giubilei F, Caltagirone C, Cercignani M. Quantitative magnetization transfer provides information complementary to grey matter atrophy in Alzheimer's disease brains. *Neuroimage* 2012;59(2):1114-1122.
39. Ridha BH, Tozer DJ, Symms MR, Stockton KC, Lewis EB, Siddique MM, MacManus DG, Rossor MN, Fox NC, Tofts PS. Quantitative magnetization transfer imaging in Alzheimer disease. *Radiology* 2007;244(3):832-837.
40. Wiest R, Burren Y, Hauf M, Schroth G, Pruessner J, Zbinden M, Cattapan-Ludewig K, Kiefer C. Classification of mild cognitive impairment and Alzheimer disease using model-based MR and magnetization transfer imaging. *AJNR American journal of neuroradiology* 2013;34(4):740-746.
41. Li X, Majumdar S. Quantitative MRI of articular cartilage and its clinical applications. *Journal of magnetic resonance imaging : JMRI* 2013;38(5):991-1008.
42. Stikov N, Keenan KE, Pauly JM, Smith RL, Dougherty RF, Gold GE. Cross-relaxation imaging of human articular cartilage. *Magnetic resonance in medicine : official journal of the Society of Magnetic Resonance in Medicine / Society of Magnetic Resonance in Medicine* 2011;66(3):725-734.
43. Sled JG, Pike GB. Quantitative imaging of magnetization transfer exchange and relaxation properties in vivo using MRI. *Magnetic resonance in medicine : official journal of the Society of Magnetic Resonance in Medicine / Society of Magnetic Resonance in Medicine* 2001;46(5):923-931.
44. Yarnykh VL. Pulsed Z-spectroscopic imaging of cross-relaxation parameters in tissues for human MRI: theory and clinical applications. *Magnetic resonance in medicine : official journal of the Society of Magnetic Resonance in Medicine / Society of Magnetic Resonance in Medicine* 2002;47(5):929-939.
45. Cercignani M, Alexander DC. Optimal acquisition schemes for in vivo quantitative magnetization transfer MRI. *Magnetic resonance in medicine : official journal of the Society of Magnetic Resonance in Medicine / Society of Magnetic Resonance in Medicine* 2006;56(4):803-810.
46. Portnoy S, Stanisz GJ. Modeling pulsed magnetization transfer. *Magnetic resonance in medicine : official journal of the Society of Magnetic Resonance in Medicine / Society of Magnetic Resonance in Medicine* 2007;58(1):144-155.

47. Ramani A, Dalton C, Miller DH, Tofts PS, Barker GJ. Precise estimate of fundamental in-vivo MT parameters in human brain in clinically feasible times. *Magnetic resonance imaging* 2002;20(10):721-731.
48. Levesque IR, Sled JG, Narayanan S, Giacomini PS, Ribeiro LT, Arnold DL, Pike GB. Reproducibility of quantitative magnetization-transfer imaging parameters from repeated measurements. *Magnetic resonance in medicine : official journal of the Society of Magnetic Resonance in Medicine / Society of Magnetic Resonance in Medicine* 2010;64(2):391-400.
49. Levesque IR, Sled JG, Pike GB. Iterative optimization method for design of quantitative magnetization transfer imaging experiments. *Magnetic resonance in medicine : official journal of the Society of Magnetic Resonance in Medicine / Society of Magnetic Resonance in Medicine* 2011;66(3):635-643.
50. Yarnykh VL. Fast macromolecular proton fraction mapping from a single off-resonance magnetization transfer measurement. *Magnetic resonance in medicine : official journal of the Society of Magnetic Resonance in Medicine / Society of Magnetic Resonance in Medicine* 2012;68(1):166-178.
51. Underhill HR, Rostomily RC, Mikheev AM, Yuan C, Yarnykh VL. Fast bound pool fraction imaging of the in vivo rat brain: association with myelin content and validation in the C6 glioma model. *NeuroImage* 2011;54(3):2052-2065.
52. Gloor M, Scheffler K, Bieri O. Quantitative magnetization transfer imaging using balanced SSFP. *Magnetic resonance in medicine : official journal of the Society of Magnetic Resonance in Medicine / Society of Magnetic Resonance in Medicine* 2008;60(3):691-700.
53. Lustig M, Donoho D, Pauly JM. Sparse MRI: The application of compressed sensing for rapid MR imaging. *Magnetic resonance in medicine : official journal of the Society of Magnetic Resonance in Medicine / Society of Magnetic Resonance in Medicine* 2007;58(6):1182-1195.
54. Gamper U, Boesiger P, Kozerke S. Compressed sensing in dynamic MRI. *Magnetic resonance in medicine : official journal of the Society of Magnetic Resonance in Medicine / Society of Magnetic Resonance in Medicine* 2008;59(2):365-373.
55. Menzel MI, Tan ET, Khare K, Sperl JI, King KF, Tao XD, Hardy CJ, Marinelli L. Accelerated Diffusion Spectrum Imaging in the Human Brain Using Compressed Sensing. *Magnetic Resonance in Medicine* 2011;66(5):1226-1233.
56. Doneva M, Bornert P, Eggers H, Stehning C, Senegas J, Mertins A. Compressed sensing reconstruction for magnetic resonance parameter mapping. *Magnetic resonance in medicine : official journal of the Society of Magnetic Resonance in Medicine / Society of Magnetic Resonance in Medicine* 2010;64(4):1114-1120.
57. Li W, Griswold M, Yu X. Fast cardiac T(1) mapping in mice using a model-based compressed sensing method. *Magnetic resonance in medicine : official journal of the Society of Magnetic Resonance in Medicine / Society of Magnetic Resonance in Medicine* 2011.
58. Sumpf TJ, Uecker M, Boretius S, Frahm J. Model-Based Nonlinear Inverse Reconstruction for T2 Mapping Using Highly Undersampled Spin-Echo MRI. *Journal of Magnetic Resonance Imaging* 2011;34(2):420-428.
59. Ji SH, Xue Y, Carin L. Bayesian compressive sensing. *Ieee T Signal Proces* 2008;56(6):2346-2356.
60. Bilgic B, Goyal VK, Adalsteinsson E. Multi-contrast reconstruction with Bayesian compressed sensing. *Magnetic resonance in medicine : official journal of the Society of Magnetic Resonance in Medicine / Society of Magnetic Resonance in Medicine* 2011;66(6):1601-1615.

61. Lustig M, Pauly JM. SPIRiT: Iterative self-consistent parallel imaging reconstruction from arbitrary k-space. *Magnetic resonance in medicine : official journal of the Society of Magnetic Resonance in Medicine / Society of Magnetic Resonance in Medicine* 2010;64(2):457-471.
62. Uecker M, Lai P, Murphy MJ, Virtue P, Elad M, Pauly JM, Vasanawala SS, Lustig M. ESPIRiT—an eigenvalue approach to autocalibrating parallel MRI: Where SENSE meets GRAPPA. *Magnetic Resonance in Medicine* 2013;n/a-n/a.
63. Weller DS, Polimeni JR, Grady L, Wald LL, Adalsteinsson E, Goyal VK. Combined Compressed Sensing and Parallel MRI Compared for Uniform and Random Cartesian Undersampling of K-Space. *2011 Ieee International Conference on Acoustics, Speech, and Signal Processing* 2011:553-556.
64. She H, Chen R-R, Liang D, DiBella EVR, Ying L. Sparse BLIP: BLind Iterative Parallel imaging reconstruction using compressed sensing. *Magnetic Resonance in Medicine* 2013;n/a-n/a.
65. Wu B, Millane RP, Watts R, Bones PJ. Prior estimate-based compressed sensing in parallel MRI. *Magnetic resonance in medicine : official journal of the Society of Magnetic Resonance in Medicine / Society of Magnetic Resonance in Medicine* 2011;65(1):83-95.
66. Chang CH, Ji J. Compressed Sensing MRI with Multichannel Data Using Multicore Processors. *Magnetic Resonance in Medicine* 2010;64(4):1135-1139.
67. Liang D, Liu B, Wang JJ, Ying L. Accelerating SENSE Using Compressed Sensing. *Magnetic Resonance in Medicine* 2009;62(6):1574-1584.
68. Liu B, Zou YM, Ying L. SparseSENSE: Application of compressed sensing in parallel MRI. *2008 International Special Topic Conference on Information Technology and Applications in Biomedicine, Vols 1 and 2* 2008:261-264.
69. Ji JX, Zhao C, Lang T. Compressed Sensing Parallel Magnetic Resonance Imaging. *2008 30th Annual International Conference of the IEEE Engineering in Medicine and Biology Society, Vols 1-8* 2008:1671-1674.
70. Stikov N, Boudreau M, Levesque IR, Tardif CL, Barral JK, Pike GB. On the accuracy of T mapping: Searching for common ground. *Magnetic resonance in medicine : official journal of the Society of Magnetic Resonance in Medicine / Society of Magnetic Resonance in Medicine* 2014.
71. Sacolick LI, Wiesinger F, Hancu I, Vogel MW. B1 mapping by Bloch-Siegert shift. *Magnetic resonance in medicine : official journal of the Society of Magnetic Resonance in Medicine / Society of Magnetic Resonance in Medicine* 2010;63(5):1315-1322.
72. Yarnykh VL. Optimal radiofrequency and gradient spoiling for improved accuracy of T1 and B1 measurements using fast steady-state techniques. *Magnetic resonance in medicine : official journal of the Society of Magnetic Resonance in Medicine / Society of Magnetic Resonance in Medicine* 2010;63(6):1610-1626.
73. Yarnykh VL. Actual flip-angle imaging in the pulsed steady state: a method for rapid three-dimensional mapping of the transmitted radiofrequency field. *Magnetic resonance in medicine : official journal of the Society of Magnetic Resonance in Medicine / Society of Magnetic Resonance in Medicine* 2007;57(1):192-200.
74. Cruz JB. System sensitivity analysis: Dowden, Hutchinson & Ross; 1973.
75. Mezer A, Yeatman JD, Stikov N, Kay KN, Cho NJ, Dougherty RF, Perry ML, Parvizi J, Huale H, Butts-Pauly K, Wandell BA. Quantifying the local tissue volume and composition in individual brains with magnetic resonance imaging. *Nature medicine* 2013;19(12):1667-1672.

76. Zhang T, Pauly J, Levesque I. Accelerating Parameter Mapping with a Locally Low Rank Constraint. In Proceedings of the 21st Annual Meeting of ISMRM 2013:p.2458.